







Evoking natural thermal perceptions using a thin-film thermoelectric device with high cooling power density and speed

Received: 15 March 2021

Accepted: 26 June 2023

Published online: 27 July 2023

 Check for updates

Luke E. Osborn  , Rama Venkatasubramanian  , Meiyong Himmmtann, Courtney W. Moran, Jonathan M. Pierce, Priya Gajendiran, Jared M. Wormley, Richard J. Ung, Harrison H. Nguyen, Adam C. G. Crego, Matthew S. Fifer  & Robert S. Armiger 

Multimodal sensory feedback from upper-limb prostheses can increase their function and usability. Here we show that intuitive thermal perceptions during cold-object grasping with a prosthesis can be restored in a phantom hand through targeted nerve stimulation via a wearable thin-film thermoelectric device with high cooling power density and speed. We found that specific regions of the residual limb, when thermally stimulated, elicited thermal sensations in the phantom hand that remained stable beyond 48 weeks. We also found stimulation sites that selectively elicited sensations of temperature, touch or both, depending on whether the stimulation was thermal or mechanical. In closed-loop functional tasks involving the identification of cold objects by amputees and by non-amputee participants, and compared with traditional bulk thermoelectric devices, the wearable thin-film device reliably elicited cooling sensations that were up to 8 times faster and up to 3 times greater in intensity while using half the energy and 1/600th the mass of active thermoelectric material. Wearable thin-film thermoelectric devices may allow for the non-invasive restoration of thermal perceptions during touch.

Receptors embedded in the skin enable us to explore our surroundings through the sense of touch and play a critical role in our ability to navigate and interact with our environment. Mechanoreceptors respond to mechanical stimulation such as pressure and vibration¹, whereas thermoreceptors, specialized free nerve endings, give rise to our perception of innocuous thermal stimuli with sensitivity to heat and cold². Restoring mechanical touch sensations including pressure^{3,4}, vibration³ and pain⁵ to an individual's phantom limb—that is, the experienced presence of a missing limb after amputation—is possible through nerve stimulation^{3,6,7} and mechanoneural interfaces⁸; however, sensations of temperature are missing despite being ubiquitous in humans. Creating advanced prosthetic limbs with rich and complex sensory inputs to the user is crucial for enhancing functionality, integration

and prosthesis acceptance^{9,10}. More broadly, multimodal sensory information is necessary for enhancing perceptual experiences and human–machine integration for prostheses, wearable, surgical and immersive extended-reality applications.

Thermoreceptor afferents conduct action potentials with a velocity of up to 15 m s⁻¹ (ref. 1,2), leading to rapid (<1 s) awareness of changes in temperature. Generating realistic and informative thermal signals on these timescales for human perception is essential for conveying real-time multimodal sensory information about the environment. For example, identifying which beverage is cold, reacting to hot objects or enhancing social connection by sensing the warmth of personal touch¹¹. In all cases, the timing of multisensory perceptions is important for promoting congruency, realism and prosthesis embodiment¹².

Developments in mechanoneural interfaces^{8,13} and sensory stimulation^{5,6,14} continue to improve a prosthesis' function^{15–17} and embodiment^{18,19}. However, current approaches cannot adequately target the small thermoreceptor fibre diameters¹, which are less likely to be activated through electrical stimulation²⁰. Although previous work has shown the re-innervation of thermoreceptor fibres after targeted sensory re-innervation (TSR) surgery to enable sensations of temperature in the phantom hand⁶, current bulk thermoelectric (TE) technologies (in particular, commercial Peltier cooling and heating devices) are unable to provide rapid thermal excitation to humans on timescales comparable to innate biological function². Also, these devices are generally not optimal for wearable systems, owing to factors such as weight and inefficient energy usage.

We hypothesized and validated that thin-film thermoelectric cooling (TFTEC) technology^{21–25} can thermally stimulate the skin and provide realistic thermal percepts faster and more intensely, compared with traditional TE technology, to effectively activate thermoreceptors, in both amputated and non-amputated limbs. In doing so, we evoked and restored thermal sensation to the phantom hand of individuals with arm amputation through targeted stimulation of the residual limb and demonstrated a closed-loop cold-object identification task. Furthermore, we found that the rate of cooling was a contributor to the perception of thermal stimuli, which was enabled by the TFTEC device. We also discovered the existence of modality-specific stimulation sites (that is, sites that respond only to thermal or mechanical stimulation) as well as mixed-modality stimulation sites (that respond to either stimulation) that created unique sensory responses in the phantom hand of amputees.

Results

To provide thermal feedback, we developed a non-invasive thermon-eural interface—between thermal stimuli and skin receptors—using a TFTEC device. The TFTEC device utilized single-crystal materials using controlled hierarchically engineered superlattice structures (CHES)²⁴ grown by metal-organic chemical vapour deposition in the p-type Bi₂Te₃/Sb₂Te₃ materials system and n-type Bi₂Te₃/Bi₂Te_{2.83}Se_{0.17} materials system (Fig. 1a–c). The TFTEC module leverages high-cooling density, and rapid and energy-efficient thermal stimulation for sensory feedback to human skin during thero-tactile tasks.

Modality-specific touch perceptions

After limb amputation, underlying nerves can re-innervate the residual limb and map to regions of the phantom limb (Fig. 1d). We mapped the residual limb of four individuals to find sites that, when mechanically or thermally stimulated, elicited sensations of touch and temperature in the phantom limb and were stable beyond 48 weeks (Fig. 1e–h and Extended Data Fig. 1). One participant underwent an unrelated surgery on their amputated limb, which affected the location of sensory perceptions; however, we were able to re-map the stimulation sites and provide thermal sensations using the new locations during a follow-up visit (Extended Data Fig. 1). In three participants (A1, A3 and A4), we observed that the stimulation sites on the residual limb were sometimes modality specific; that is, thermal activation did not always elicit sensations in the phantom hand in the same location as mechanical activation (Fig. 1e,g,h). For instance, in participant A1, one particular region of the skin mapped to the phantom wrist when thermally stimulated but was mapped to the phantom little finger when mechanically stimulated (Fig. 1e). This observed modality specificity implies re-innervation of mechanoreceptors from one nerve fascicle in the same location as thermoreceptors from another fascicle, suggesting the presence of modality-specific re-innervation of skin receptors.

Participants A1 and A4 had previously undergone sensory mapping using mechanical and electrical stimulation^{15,26,27} but had not reported thermal sensations until a thermoelectric cooling (TEC) device was used on the targeted sites of the residual limb (Fig. 1e–h). Thermal and

mechanical stimuli applied to the residual limb were perceived on the skin itself except for the mapped sites, which were perceived as thermal or pressure sensation in the phantom hand (Fig. 1e–h, Supplementary Video 1 and Supplementary Video 2). Although only A4 had undergone TSR surgery, all participants were able to perceive thermal sensations in their phantom hand, showing that TSR is not required to restore thermal sensations.

Rapid and efficient TFTEC device response

To enable rapid and realistic perceptions of thermal stimulation, we fabricated a TFTEC device with thermal responses capable of driving a perceptible thermal difference on a biologically relevant timescale^{28,29}. The speed of cooling to a target temperature is important because of reported perceptual thresholds of 1 °C over 250 ms (ref. 29), and it is known that rate is proportional to thermoreceptor response³⁰ and perceived intensity²⁹. TFTEC devices offer benefits over traditional bulk materials TEC devices by nature of their faster cooling speeds and enhanced cooling power density^{31,32}, making them well suited for sensory feedback applications such as conveying information of a cold object during grasping with a prosthesis.

The TFTEC device was fabricated using metal-organic chemical vapour deposition to grow 25-µm-thick p-type (Bi₂Te₃/Sb₂Te₃) and n-type (Bi₂Te₃/Bi₂Te_{2.83}Se_{0.17}) CHES materials^{21,24,31} then transferred to an aluminium nitride (AlN) substrate (Fig. 2a and Extended Data Fig. 2). Each thin-film die was 1.0 mm × 0.6 mm × 0.3 mm and consisted of two p–n couples with an AlN header connecting the p–n couples (Fig. 2a,b and Extended Data Fig. 2). Each of the p–n couples were thermally and electrically in parallel for built-in redundancy, but each of these couples were in a series electrical circuit of a 3 × 4 (or 12-couple) module. We fabricated a 3 × 4 p–n couple array on an AlN substrate (Fig. 2c,d) to achieve cooling over the area of interest. The couples in the array were connected electrically in series using gold (Au)-coated copper (Cu) traces on the AlN substrate. Each p–n couple was sandwiched between AlN headers and connected electrically in series using contact metallization of the CHES semiconductors (Fig. 2e), but the thin-film couples were thermally connected in parallel by placing a common SiC header on top of the 3 × 4 array. The entire packaged array was approximately 1.2 mm in height (Fig. 2f and Extended Data Fig. 2).

The TFTEC offers high cooling power density, which is needed to evoke an effective cooling response, due to equation (1) (ref. 31)

$$q_{\max} = \frac{1}{l} \left\{ \left[\left(\frac{1}{2} \frac{\alpha^2 T_c^2}{\rho} \right) \right] - [k(T_h - T_c)] \right\} \quad (1)$$

where q_{\max} is the maximum cooling power density, and l is the thickness of the active TE material in a device (see Supplementary Methods for full derivation). T_c is the cold-side (skin) contact temperature, α is the Seebeck coefficient, ρ is the resistivity of TE material, k is the thermal conductivity of the material and T_h is the heat-rejection temperature. Previous work showed cooling density advantages with a TFTEC device for cooling microprocessors for a given temperature differential ($T_h - T_c$)³¹; here we leverage a similar advantage to evoke thermal sensations using a TFTEC device with improved CHES thin-film materials.

For similar ρ , T_h and T_c , the q_{\max} is higher in TFTEC devices, compared to conventional TE devices. This difference in q_{\max} is largely due to the reduction of l and, to a smaller extent, lower k for about the same α and ρ , due to the higher TE figure of merit (ZT) in CHES materials^{21,24,31} (Supplementary Methods and Extended Data Fig. 3).

The reduction in l also gives a key advantage in the intrinsic cooling speed of TFTEC devices²¹, which is important for evoking strong thermal perceptions²⁹, stemming from the active TE response time (τ) given by equation (2)

$$\tau \sim 4l^2/\pi^2D \quad (2)$$

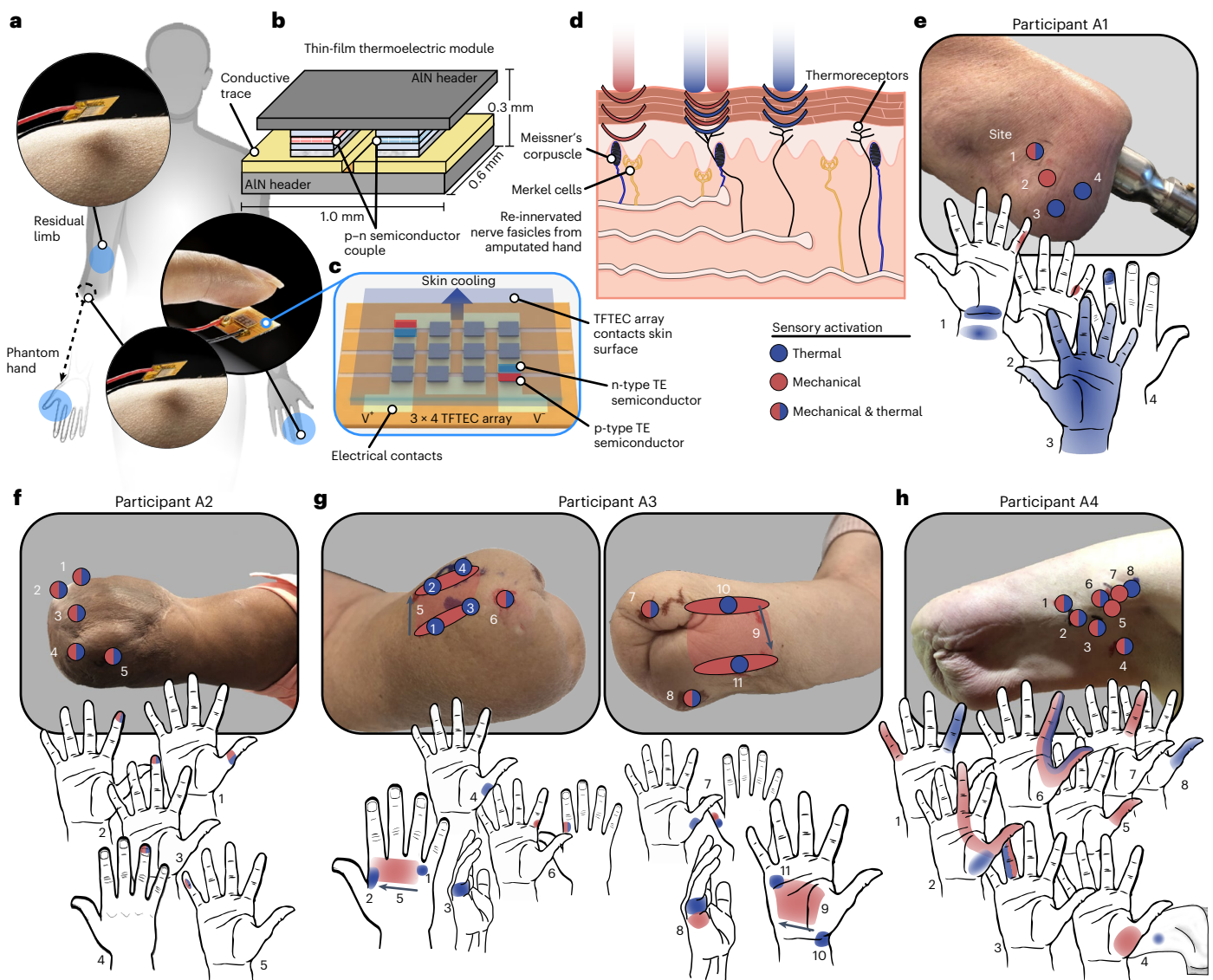


Fig. 1 | Mapping thermal sensations in the phantom hand. **a**, After limb amputation, perception of the phantom hand persists. Non-invasive thermal stimulation of the skin was used to create thermal sensations in the phantom hand, residual limb and intact fingertips (blue areas). **b**, We used a rapid-response TFTEC device, composed of p-type and n-type CHESS thin-film TE materials, to restore thermal sensations. **c**, A common header connected the TFTEC modules thermally in parallel and contacted the skin to provide localized cooling, which was perceived in the phantom hand when targeting specific skin sites. **d**, Receptors in the skin respond to physical touch (Meissner's corpuscle and Merkel cells), whereas thermoreceptors (free nerve endings) respond to temperature. Stimulation on the skin surface propagates to activate the underlying receptors and nerves. Nerve re-innervation after amputation enables stimulation of sites

on the skin to create sensations in the phantom hand. Nerve fibres from different fascicles can re-innervate the same region of skin, leading to modality-specific responses in different regions of the phantom hand. **e–h**, Sites on the residual limbs of individuals (participant A1 (**e**), participant A2 (**f**), participant A3 (**g**) and participant A4 (**h**)) with arm amputation that, when stimulated, elicit sensory perception in the phantom hand. Stimulation sites were generally up to 1 cm in size. Mapped sites generated thermal percepts via thermal stimulation on the residual limb (blue). Physical touch in some locations (red) also elicited tactile sensations but sometimes in different regions of the phantom hand when compared to thermal stimulation, showing the presence of spatially collocated re-innervation of modality-specific receptors from different nerve fascicles.

where l is the thickness of the TE element and D is the thermal diffusivity. These underlying relations are dependent on inherent material properties, but the actual device performance can be influenced by other factors beyond the active TE components. For example, actual device response time is increased due to other thermal parasitic effects, such as thermal resistance between the device and human skin as well as the active TE device and passive parts (for example, AlN) and its heat-rejecting surface. Given the effective module properties (Extended Data Fig. 3), the higher intrinsic speed of the TFTEC device translates to higher cooling speed (Fig. 2g,h), which is beneficial for human skin stimulation when delivering feedback regarding an object's

temperature. The combination of higher cooling power density (q_{\max}) and smaller τ apparently leads to a direct cooling advantage, in terms of energy used to reach a target temperature (Fig. 2i), for the thin-film CHESS devices^{24,31,32}.

The overall TFTEC device is a thin (~1.2 mm) and lightweight (mass = 0.05 g, Extended Data Fig. 2b) 'refrigeration' device that can provide cooling of 10–20 °C below ambient in ~3 s and hold this thermal gradient for extended durations, while also being in a wearable form factor and enabling reliable thermotactile perceptions. This fast, intense cooling near room temperature can be used to provide spatially and temporally realistic thermal stimulation to human skin.

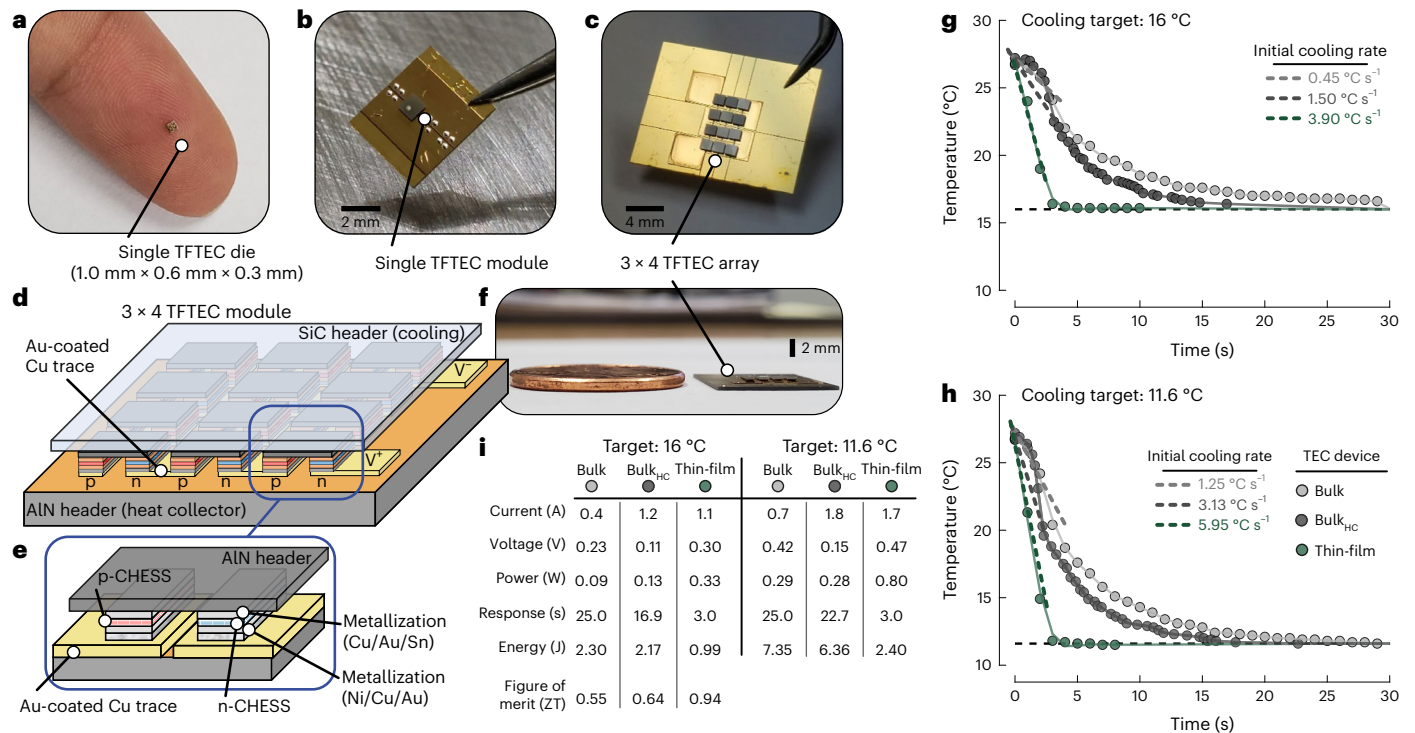


Fig. 2 | Thin-film TE-device cooling and energy consumption. **a**, A single TFTEC die (1.0 mm × 0.6 mm × 0.3 mm), **b**, mounted on an AlN backplate, and **c**, a 3 × 4 array of TFTEC dies used for skin stimulation. **d**, Individual TFTEC dies were mounted and connected electrically in series such that current flowed into all the couples to create the uniform cooling effect. **e**, Each module contained p-type and n-type CHESS semiconductors with contact metallization and Au-coated Cu traces to enable current flow between modules. AlN substrates acted as the heat collector (bottom) and cooling surface (top) for thermal transfer to human skin during contact. **f**, The TFTEC array with thickness of 1.2 mm and mass of 0.05 g (right) compared to a US one-cent coin (left). **g**, Cooling to 16 °C and **h**, 11.6 °C for

traditional bulk, bulk_{HC} and TFTEC modules during benchtop tests. The bulk_{HC} device uses an operating current similar to the TFTEC device; however, the TFTEC device responded within 3 s compared to the traditional bulk devices, which required more than 16 s. The initial cooling rate, calculated over the first 2 s, for the TFTEC device was 3.90 °C s⁻¹ and 5.95 °C s⁻¹ for the 16 °C and 11.6 °C targets, respectively. **i**, For the same target temperature, the TFTEC device was 4.8 to 8.7 and 2.7 to 3.05 times faster than the bulk and bulk_{HC} devices, respectively, and consumed up to 3 times less energy while also having a higher module-level ZT (Extended Data Fig. 3). The energy consumed to reach 16 °C was 2.30 J and 2.17 J for both bulk TEC devices and was 0.99 J for the TFTEC device.

The low-profile and lightweight nature of TFTECs make them suitable for skin surface applications without weight or volumetric hindrances affecting movement.

The TFTEC device was faster in achieving steady-state target temperatures compared to both traditional bulk and high-capacity bulk (bulk_{HC}) TEC devices (Fig. 2g,h). Notably, the thin-film device reached the target temperature within ~3 s, whereas the bulk devices required at least ~17–25 s. The steady-state responses of the TEC devices, once they reached the target temperature, were stable with no observable deviation from the set point, which is important for skin stimulation (Extended Data Fig. 3a,b). The energy consumed to achieve the target temperatures was 2.1–3.1 times lower for the thin-film device (0.99 J and 2.4 J for 16 °C and 11.6 °C, respectively) compared to the bulk devices (Fig. 2i). An extended characterization of the TFTEC device showed long-term repeatability in both benchtop (400 min) and human perception tests (180 min) (Extended Data Fig. 4).

The higher operating power (0.3–0.8 W, Fig. 2i) for the TFTEC device to achieve a 10–15 °C change in temperature is consistent with the higher cooling power density relative to bulk devices. However, due to the faster response and higher device ZT (that is, for converting input electric power to cooling power), the actual energy consumed is smaller for the TFTEC device for achieving a target thermal stimulation (Fig. 2i). Despite offering a higher capacity for cooling and active TE area, the bulk_{HC} module's ZT (0.64) is more similar to the standard TEC device (0.55) in contrast to the CHESS TFTEC device (0.94) (Fig. 2i and Extended Data Fig. 3). Previous work has also shown improved

conversion efficiency and power density in similar thin-film modules compared to the bulk_{HC} module²⁵. Increasing the capacity of the bulk TEC device and operating current improved speed slightly (Fig. 2g,h) but did not substantially change the energy consumed to achieve the target temperature (Fig. 2i, Extended Data Fig. 3 and Supplementary Methods). The fully packaged 3 × 4 array is well suited for a variety of wearable and thermotactile applications due to its small form factor, lending itself well to integration in systems such as clothing, prostheses or even medical bandages for wound thermal regulation (Supplementary Discussion).

Faster and stronger phantom thermal perceptions

We demonstrated the thermotactile use of the TFTEC device by placing it on the skin of the four participants with amputation to restore thermal sensation in the phantom hand (Fig. 3a). The objective was to evaluate the effectiveness of the thin-film device in creating perceived cooling when stimulating to a target temperature, which is important for sensory feedback. On each trial, the cooling target was set to 16 °C, starting from room temperature (~22–25 °C).

Compared to the standard bulk TEC device driven to the same target temperature, participants perceived thermal cooling more often when the TFTEC device was used to provide thermal stimulation ($P < 0.05$ for A1 and A3) (Fig. 3b). Thermal stimulation was applied to at least two different sites on each participant to elicit thermal sensations in either the residual or the phantom limb (Fig. 3a,b and Supplementary Video 3). Sensations in the phantom hand were elicited by thermal

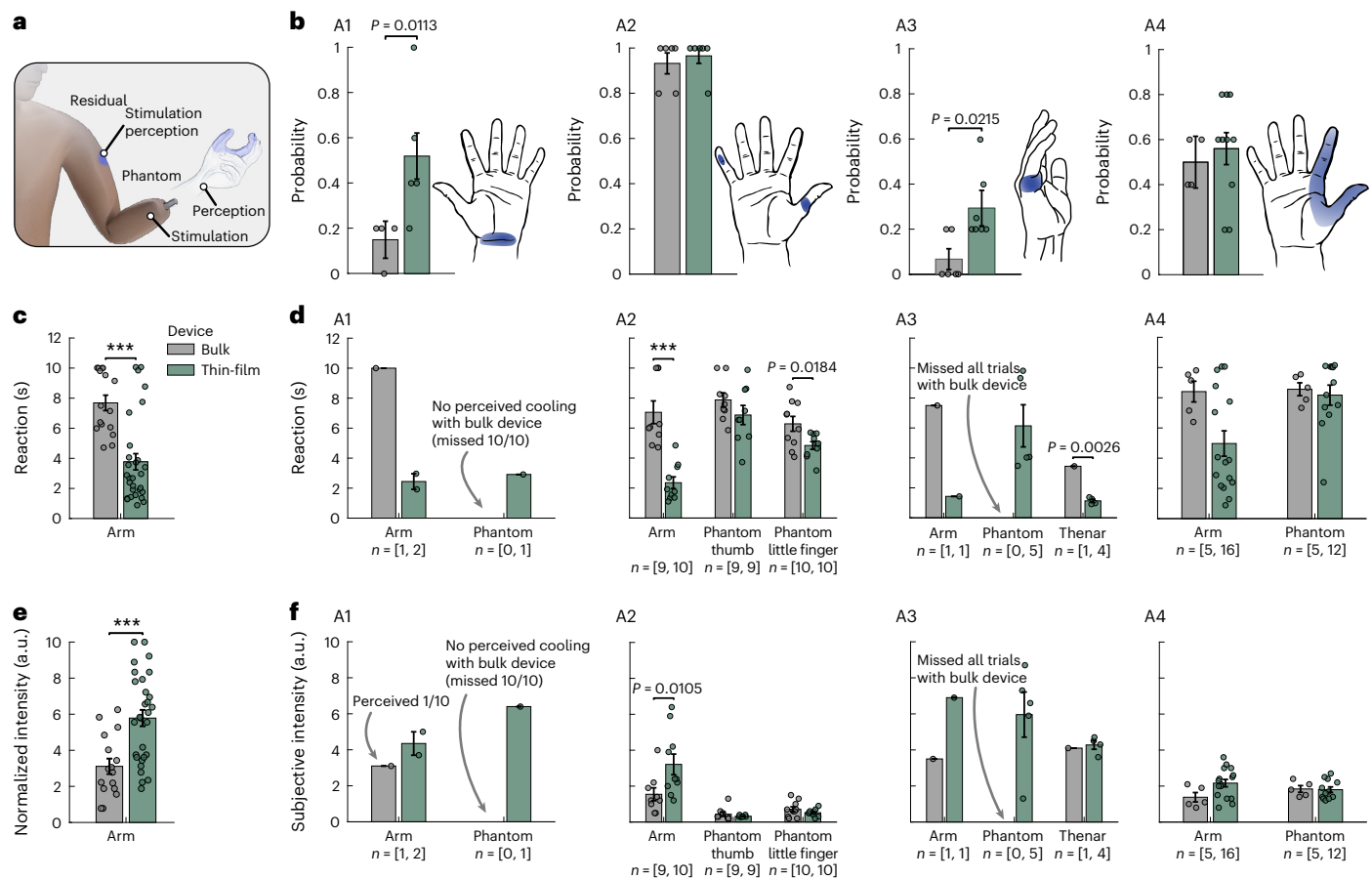


Fig. 3 | Rapid thermal perception in the phantom limb with TFTEC device.

a, Thermal sensations were delivered to either the phantom limb or the residual limb through skin stimulation in four amputees. **b**, Each participant received thermal stimulation to a unique part of their phantom limb or residual limb and were more likely (A1, A3, $P < 0.05$) to feel the thermal sensation using the TFTEC device. Data presented as performance per block of up to five independent trials. A1: $n = 20$ trials (4 blocks, bulk), 25 trials (5 blocks, TFTEC); A2: $n = 30$ trials (6 blocks, bulk and TFTEC); A3: $n = 30$ trials (6 blocks, bulk), 34 trials (7 blocks, TFTEC); A4: $n = 20$ trials (4 blocks, bulk), 50 trials (10 blocks, TFTEC). **c**, Perceptual onset of thermal sensation was captured by measuring the reaction time of participants when a temperature change was perceived. The reaction time to thermal onset on the arm, when combined across all participants, was faster for the TFTEC device (median = 2.7 s, $n = 29$ independent trials) compared to the bulk device (median = 7.3 s, $P < 0.001$, $n = 16$ independent trials). **d**, In general, thermal activation with the TFTEC device resulted in faster perception of the thermal sensations in the residual limb and phantom hand. In some cases, the bulk device did not elicit any thermal sensations in the phantom limb (A1 and A3).

e, The perceived thermal intensity, rated using a subjective scale and normalized to the maximum value reported for each participant, between bulk and TFTEC devices. When normalized across participants during arm stimulation, the TFTEC device was perceived as twice as intense (median = 5.8, $n = 29$ independent trials) as the bulk device (median = 2.9, $P < 0.001$, $n = 16$ independent trials). **f**, For each participant, perceived intensity on the phantom limb was similar across devices, except A2 ($P = 0.0105$); however, the bulk device only produced thermal sensations in the phantom limb for half of the participants, whereas the thin-film device elicited sensations for all participants. **d, f**, The number of independent trials for each condition that elicited thermal perception is given by n . Total number of independent trials, including those that did not elicit thermal perception, for each condition was 10 (A1, A2), 9 (A3 arm TFTEC), 10 (A3 thenar), 15 (A3 arm bulk, A3 phantom TFTEC), 10 (A4 bulk) and 25 (A4 TFTEC). **c–f**, Data represent independent trials. The target cooling temperature was set to 16 °C for all trials. **b–f**, Bars represent mean \pm s.e.m. of individual trials. P values were generated with a two-sided Mann–Whitney U -test and only if thermal sensation was perceived for at least three trials at a given location. $***P < 0.001$.

stimulation on the previously mapped sensory locations (Fig. 1e–h). To measure the speed of thermal perception, participants pressed a button as soon as they perceived a change in thermal sensation (Fig. 3c,d, Supplementary Fig. 1 and Extended Data Fig. 5). To elicit sensations on the residual limb, the TEC device was placed at a location that generated thermal sensations at the site of stimulation (that is, the arm itself).

Importantly, the TFTEC device elicited sensations of cooling in the phantom limb of all participants, whereas only half of the participants perceived thermal sensation when using the bulk device (A2 and A4) (Fig. 3d,f).

In addition to being more likely to perceive thermal sensations with the TFTEC device, participants perceived the thermal sensations faster when stimulation was perceived in their arm ($P < 0.001$) or phantom limb ($P < 0.01$ for A2 and A3) compared to the standard bulk device

(Fig. 3c,d). The thermal intensity was also significantly greater when perceived on the arm ($P < 0.001$, Fig. 3e and Supplementary Video 1). However, differences in perceived intensity were not as prominent in the phantom limb across each individual (Fig. 3f), although reports from participant A2 show differences in quality with the thin-film device being perceived as a more naturalistic sensation (Supplementary Video 1). The lack of thermal perception from the bulk device, along with faster and stronger perceptions from the TFTEC device, suggests that the rapid and targeted thermal changes from the TFTEC device are critical aspects for reliably eliciting thermal sensations.

Participant A4 also performed the experiment with the bulk_{HC} device, although it did not provide significant differences from the TFTEC device other than in a few trials on the phantom limb (Extended Data Fig. 6 and Supplementary Discussion). Notably across all devices,

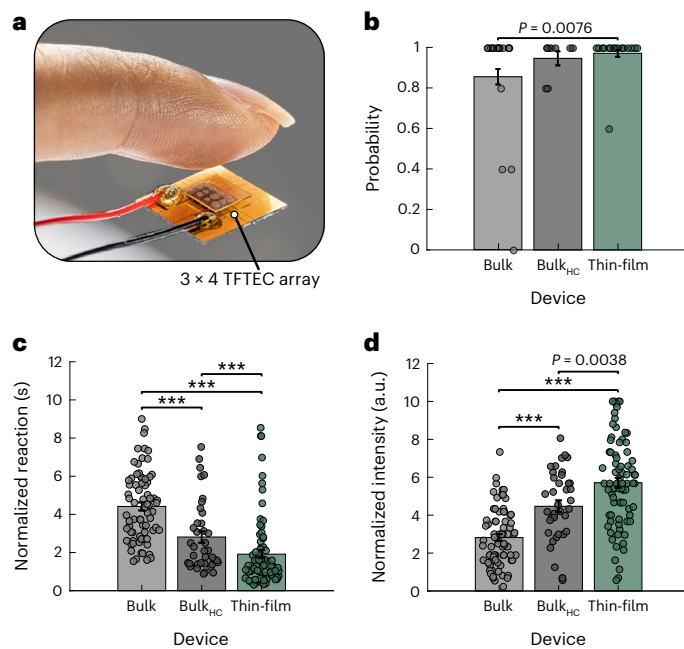


Fig. 4 | Performance and perception with the TFTEC array exceeds that of the high-capacity bulk device. **a**, Fingertip thermal stimulation on four non-amputee participants. **b**, Probability of detecting thermal cooling with standard bulk, bulk_{HC} and TFTEC devices. Data presented as performance per block of five independent trials, $n = 85$ trials (17 blocks, bulk), 40 trials (8 blocks, bulk_{HC}) and 80 trials (16 blocks, TFTEC). **c**, Reaction to perceived cooling was faster for the TFTEC (median = 1.3 s, $n = 78$ independent trials) than for the bulk ($P < 0.001$, median = 4.3 s, $n = 73$ independent trials) and bulk_{HC} ($P < 0.001$, median = 2.1 s, $n = 38$ independent trials) modules. The reaction time was normalized by subtracting the mean visual reaction time for each participant. **d**, Similarly, the TFTEC was perceived as more intense (median = 5.7) than the bulk ($P < 0.001$, median = 2.7) and bulk_{HC} ($P = 0.0038$, median = 4.4) modules. Intensity was normalized to the maximum reported intensity for each participant. Data are presented from individual trials. Bars represent mean \pm s.e.m.; P values were generated with a two-sided Mann–Whitney U -test. *** $P < 0.001$.

A4 reported warming sensations on some trials, although stimulation was set to 16 °C (Extended Data Fig. 6). These contrasting perceptions are likely caused by the slow thermal changes being sometimes described as ‘tingling’ sensations by this participant as well as A2 (Supplementary Video 1). Other explanations include the underlying nerve fibres being responsive to both warming and cooling in this participant, leading to difficulty differentiating between subtle changes in temperature (Supplementary Discussion). The other participants reported sensations of cooling; however, most participants noted that the bulk device produced more of a ‘tingling’ sensation as it began to change temperature but that the TFTEC device was often more a ‘cold’ sensation (Supplementary Video 1). This difference in perceptual quality is important to note and, because thermoreceptor activity is correlated with the rate of temperature change²⁹, is likely driven by the faster cooling rate and cooling power density of the thin-film device (Fig. 2g–i).

Faster and stronger fingertip thermal sensations

We also performed thermal stimulation to the right index finger in four other participants without arm amputation (Fig. 4a and Supplementary Video 4). In two of the participants with no limb difference, we also evaluated the bulk_{HC} device given its higher capacity for cooling and similar operating current to compare with the TFTEC technology. The participants were more likely to perceive a thermal sensation with the TFTEC device compared to the standard bulk device (Fig. 4b and Extended Data Fig. 7). Similar to the results with amputee participants,

the reaction time to thermal onset was reduced with the TFTEC device compared to both the high-capacity and the standard bulk devices (Fig. 4c). The perceived cooling intensity was also higher for the TFTEC device compared to both the high-capacity and standard bulk devices (Fig. 4d). Despite the bulk_{HC} module having the highest active TE area (a), aspect ratio (a/l) and thermal conductance (Extended Data Fig. 3g), the perceptual response to thermal stimulation was still faster and stronger for the TFTEC device due to its higher ZT and faster response time (Fig. 2i and Extended Data Fig. 3).

In essence, we found that the TFTEC device enabled more reliable, faster and stronger thermal sensations in the phantom limb compared to bulk TEC stimulation (Fig. 3) and outperformed the bulk_{HC} device during fingertip stimulation with non-amputee participants (Fig. 4), showing the value for use in human sensory feedback applications.

Thermal perception to identify cold objects

Going beyond benchtop and perceptual detection experiments, we also demonstrated a closed-loop functional task in which a user identified the location of a cold object using thermal feedback. Wearing an advanced prototype Modular Prosthetic Limb (MPL)³³ equipped with infrared temperature sensors, an amputee participant (A1) grasped objects at different temperatures to feel a cold object via a TFTEC device placed on the residual limb (Fig. 5a,b and Supplementary Videos 5 and 6). Participant A1, who received real-time thermal feedback to the phantom limb during prosthesis control, was successful in feeling and identifying the correct cold object on every trial over the course of 2 days during a follow-up visit (Fig. 5c).

Further evaluating the potential impact of thin-film TEC technology during real-time functional tasks, we performed an additional experiment using a virtual environment. Participants controlled a virtual Modular Prosthetic Limb (vMPL) to touch virtual objects and identify the ‘cold’ one (Fig. 5d, Supplementary Videos 7 and 8 and Extended Data Fig. 8). Participant A1 performed the task with all three TEC devices and was significantly better at completing the task with the TFTEC device compared with the bulk device; interestingly, participant A2 was only successful during trials with the TFTEC device, further demonstrating the value of fast cooling performance in evoking useful thermal percepts (Fig. 5e). Although the task success for A1 was only 29% greater with the TFTEC device compared with the high-capacity bulk device, the time spent ‘touching’ each virtual object during the trials was reduced when using the TFTEC device (Fig. 5f). The reduction in time to determine object temperature (using the TFTEC device) implies faster identification of a cold object and could enable future real-time control tasks with faster motor adaption due to the more certain sensory input provided by the TFTEC device^{34,35}. Reduced object touch time was replicated in two non-amputee participants who also performed the virtual cold-object identification task (Extended Data Fig. 8d–f).

Discussion

The unique combination of fast-rate TE cooling non-invasively applied to re-innervated sensory sites enabled the restoration of thermal sensation to the phantom hands of individuals with arm amputation. This discovery shows that underlying sensory fibres re-innervate after amputation, as shown previously^{6,15,26}, but we also observed that modality-specific receptor structures for mechanical and thermal inputs are preserved and can re-innervate the same region of the skin despite being from nominally different fascicles and representing different parts of the phantom hand (Fig. 1e–h). This observation that thermal and mechanical skin stimulation sites may or may not be co-located and may or may not map to the same region of a user’s phantom limb creates opportunities for planning multi-modality haptic feedback and flexibility in locating physical devices.

Importantly, our results show that TSR surgery is not necessarily required to restore thermal sensations in the phantom hand⁶, and these sensations are stable beyond 11 months (A2, Extended Data Fig. 1),

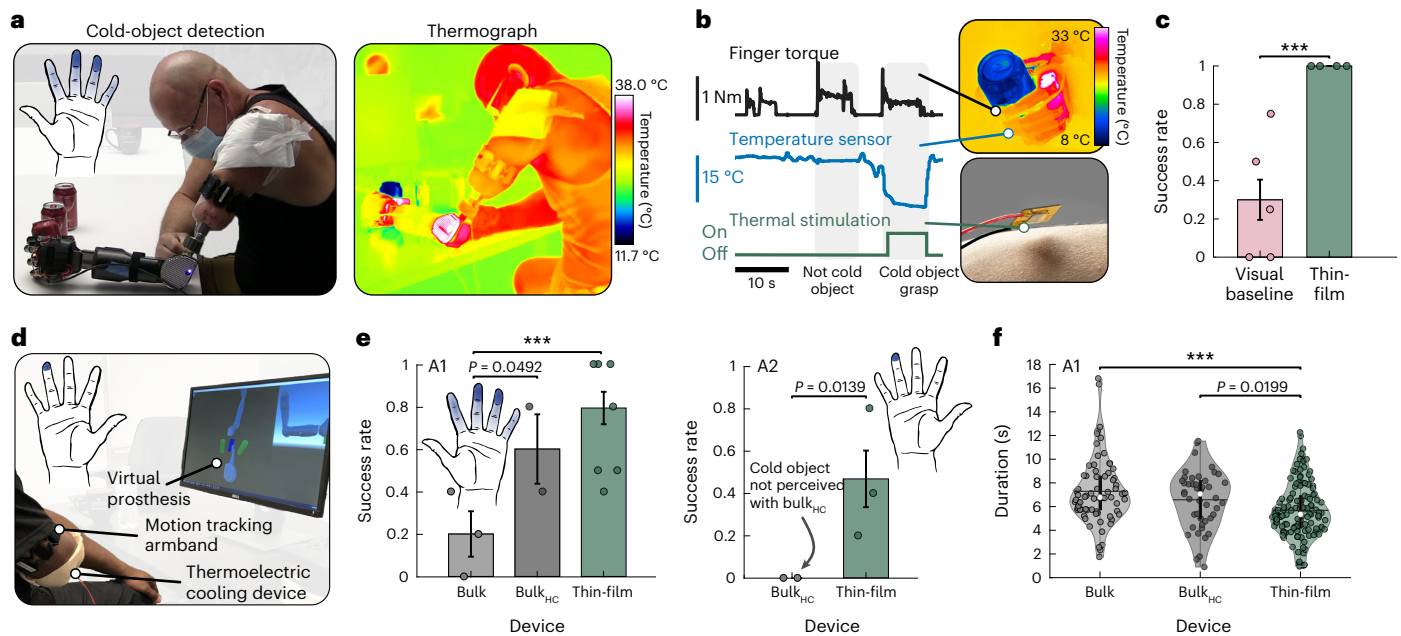


Fig. 5 | Restored thermal sensation during functional tasks. **a**, One participant (A1) performed a cold-object detection task with their prosthesis while receiving thermal sensory feedback to the phantom hand. **b**, During the object detection task, an infrared temperature sensor was embedded in the fingertip of the prosthesis and the signal was used to determine when a cold object was being grasped, which in turn activated the thermal stimulation on the skin for real-time feedback. **c**, During testing over 2 days, the participant was able to identify the cold object (within three total objects) on all trials, which was significantly more accurate than chance using only visual information. Data represent performance of each block, which contains up to five independent trials; $n = 20$ trials (4 blocks, visual baseline) and 19 trials (4 blocks, TFTEC). **d**, Two participants (A1, A2) also performed a virtual cold-object detection task in which they controlled a virtual prosthesis to touch virtual objects, one of which was cold. **e**, The participants were more successful in identifying the virtual cold object when receiving thermal stimulation from the TFTEC device (A1: 0.77, A2: 0.47), compared to

traditional bulk TEC technologies (A1: bulk = 0.20, bulk_{HC} = 0.60; A2: bulk_{HC} = 0). Participant A2 was only successful in identifying the correct object when using the TFTEC device but not the bulk_{HC} device. Data represent performance per block of up to five independent trials; $n = 15$ trials (3 blocks, A1 bulk, A2 TFTEC), 10 trials (2 blocks, bulk_{HC}) and 31 trials (7 blocks, A1 TFTEC). **f**, The time spent touching each object to detect its temperature in the virtual environment was significantly reduced for A1 when using the TFTEC device (median = 5.3 s, $n = 125$ independent touches over 31 trials) compared to the bulk (median = 6.8 s, $n = 71$ independent touches over 15 trials) and bulk_{HC} (median = 7.1 s, $n = 45$ independent touches over 10 trials) devices (Extended Data Fig. 8). **d, f**, Bars represent mean \pm s.e.m. of individual trials; **f**, violin plot whiskers represent the minimal and maximal values, the vertical lines indicate the first and third quartiles, the horizontal lines are means, and the white dots are the medians; P values were generated with a two-sided Mann–Whitney U -test. *** $P < 0.001$.

which offers great promise for creating complex multimodal sensory perception in a broad range of prosthesis users. Sensations were perceived as originating from the phantom when mapped sites were stimulated, suggesting either that the local thermoreceptors in the residual limb were inactive or that the revived thermal sensation in the phantom hand was so pronounced that any thermal sensation localized to the residual limb was perceptually ignored.

In addition to long-term cooling functionality over several hours when worn on the fingertip (Extended Data Fig. 4), we demonstrated restored functionality to amputees during closed-loop thermal detection tasks, both physical and virtual. Importantly, in one amputee participant only the TFTEC device was able to restore closed-loop thermal perception functionality during the virtual object detection task (Fig. 5e). Despite CHES TFTEC device technology being in the research prototype phase, compared to mature bulk devices, the device was successfully integrated into a prosthesis and used over 2 days to complete a cold-object identification task. Further, results from the virtual object identification task were reproduced with non-amputee participants, suggesting broader applicability of TFTEC devices for enhancing sensory feedback. Improved device packaging could further enhance device robustness and enable application in chronic wearable electronics and robotic systems for human–machine interfacing applications requiring rapid and accurate thermal transfer, such as measuring perceptual abilities after injury, or low-profile thermal regulation of implanted electronics. The TFTEC device steady-state response is also capable of long-term water freezing from the atmosphere—showing

functionality for open-air applications, such as in cauterization and other thermal functionalities at skin sites during surgery (Supplementary Discussion, Supplementary Fig. 2 and Supplementary Video 9).

Traditional bulk TEC devices can provide skin thermal feedback^{36–38}, and recent work showed increasing efficiency³⁹ and flexibility⁴⁰ for wearable applications; however, an important aspect of thermal feedback is matching the biological timescales of nerve fibre responses to achieve a target temperature, which is essential for creating realistic and temporally meaningful sensory perception feedback. The TFTEC device was able to cool at nearly $6\text{ }^{\circ}\text{C s}^{-1}$ when set to a target of $11.6\text{ }^{\circ}\text{C}$ (Fig. 2), which is critical for creating rapid thermal perception in humans²⁹.

Previous work showed that a decrease of $1\text{ }^{\circ}\text{C}$ can be detected during skin cooling and that a cooling rate of $4\text{ }^{\circ}\text{C s}^{-1}$ is perceived as being twice as intense as a cooling rate of $0.5\text{ }^{\circ}\text{C s}^{-1}$ given the same target temperature²⁹. In our results, this perceived difference in cooling intensity, based on rate, was replicated in both amputee and non-amputee participants feeling the faster TFTEC device cooling ($3.9\text{ }^{\circ}\text{C s}^{-1}$) as being around twice as intense as the bulk TEC device cooling ($0.45\text{ }^{\circ}\text{C s}^{-1}$) (Figs. 3e and 4d). The cortical response of skin thermal stimulation happens before the steady-state value is reached and occurs within several hundred milliseconds⁴¹, reiterating the importance of change in temperature rate for eliciting useful thermal percepts. However, achieving this rate of cooling and thermal perception is a function of both the device and skin interface. TFTEC modules can intrinsically respond even as quickly as tens of microseconds²¹ without the AIN

and SiC contact headers, and other microstructured TE devices have been shown to cool within 1 ms (ref. 42). The addition of AlN and SiC headers, which allow for better contact with skin and prevent damage to the TFTEC module during repeated placement on the human body, inherently introduces delays in thermal transfer to the skin; however, they still enable rapid delivery of cooling sensation (Fig. 2g). Because the human body is transmitting and perceiving thermal information within hundreds of milliseconds, quickly generating a change in temperature (ΔT) of 1 °C is critical for eliciting fast thermal percepts in humans. We observed $\Delta T = 1$ °C in -256 ms (3.9 °C s⁻¹) and -168 ms (5.95 °C s⁻¹) with the TFTEC device for steady-state targets of 16 °C and 11.6 °C, respectively (Fig. 2g,h). Although the TFTEC module reached the steady-state target temperature after 3 s, the normalized reaction to cooling sensation occurred in as little as 313 ms (median: 1.3 s, Fig. 4c). For future wearable applications, optimizing the TFTEC device packaging such as reduced header thicknesses could help further reduce the effective response time even.

Because of the compactness, reduced energy consumption, cooling power density and speed of the TFTEC device, future multimodal sensory-feedback technology may integrate pressure-inducing mechanical actuators with thermal thin-film TE devices or other TE technologies^{22,23,40,43–46} to elicit a complex array of thermotactile sensory stimulations. Future TFTEC device advancements, including packaging, could enable enhancements to cooling efficiency, cooling power density and speed of thermal stimulation for reduced battery-power consumption and for translational applications. Although translation to future human-machine applications includes challenges such as system power management and integration of TFTEC modules on flexible substrates, here we have shown a non-invasive thermoneural interface capable of providing sensations of temperature to the phantom limb. More broadly, the TFTEC device enabled enhanced perceptual qualities and speed of thermal sensations in humans. These results have implications for use in human-machine interfaces and other areas such as immersive mixed reality, wearables⁴⁰, mapping thermal-mediated neural circuits⁴⁷, diagnosing sensory symptoms after stroke⁴⁸ and advanced wound care⁴⁹.

Methods

This research protocol was reviewed and approved by the Johns Hopkins Medicine Institutional Review Boards in accordance with all applicable Federal regulations governing the protection of humans in research. All participants provided written informed consent to participate in the study. Participants were compensated up to \$15 h⁻¹ in gift cards, or if participants were Johns Hopkins University Applied Physics Laboratory (JHU/APL) employees, then they were given a project budget to cover their time for performing the experiments.

Participant recruitment

Four participants with arm amputation were recruited for this study (A1–A4, 2 males, 2 females, 41–65 years old at study onset). Participant A1 (male) had a left transhumeral arm amputation, had previously undergone targeted muscle re-innervation surgery and was previously implanted with an osseointegrated interface⁵⁰. Participant A1 had undergone sensory mapping of his residual limb to activate the phantom hand using both mechanical and electrical stimulation^{15,26}. Participants A2 (male) and A3 (female) both had right transradial amputations, and A4 (female) had a right transhumeral amputation with TSR surgery^{6,51} and had previously undergone sensory mapping with non-invasive electrical stimulation²⁷. Participant A3 also had a partial hand amputation on her left side, which was an additional site used for the thermal stimulation testing (Fig. 3b).

Participant A1 underwent an unrelated surgical procedure on his left arm in between his initial sensory mapping and thermal perception experiments and his return for a 2 day follow-up visit to conduct additional experiments, approximately 29 months (128 weeks) after his initial visit. The unrelated surgery affected the location of

his sensory stimulation sites (Extended Data Fig. 1); however, we were able to re-map the phantom limb, demonstrating the robustness and applicability of our approach to a broad population of individuals and amputation conditions. Participant A2 returned for a follow-up visit to conduct additional experiments, approximately 11 months after the initial sensory mapping and thermal perception experiments.

Six additional participants without amputation and without sensory deficits were also recruited for the study (B1–B6, 3 males, 3 females, 20–30 years old at study onset). All participants provided written informed consent to be a part of this study and have their images taken and used for publication.

Thin-film TE cooling device fabrication

The fabrication of the TFTEC cooling module utilizing the higher-performance single-crystal CHES materials²⁴ is shown in Extended Data Fig. 2. The full details of the material properties and advantages in terms of TE device ZT over conventional bulk materials as well as superlattices are described in previous work^{21,24,25,31}. To fabricate the TFTEC devices: (1) two separately grown p-type and n-type CHES thin films (25 μm) were grown on GaAs substrates followed by Cu (30 μm) and Au (1 μm) contact metallization (total thickness 31 μm); (2) the p- and n-CHES materials were then turned into strips and diced. Following the previous step, the p- and n-strips were bonded onto a secondary AlN substrate (header 1, 380 μm) using a Sn preform or plated Sn (20 μm), and then the GaAs substrate was selectively removed. After this step, (3) another layer of metallization (Ni/Cu/Au, 30 μm) was carried out, and the individual p–n couples were attached to indium solder pads (25 μm) on a Cu trace (30 μm) on an AlN substrate (header 2 that became the heat collector, 380 μm). Next, (4) several such p–n couples were assembled with a common heat-collecting or cooling surface, which in this case was a transparent SiC layer (330 μm). The total thickness of the module was approximately 1.2 mm. The thickness of two AlN headers was 380 μm each and contained a <1 μm pre-metallization layer of Ti/Pt/Au. The rest of the electroplated metallization layers (combined 61 μm), Sn bonding layer (20 μm), In solder (25 μm) and the active CHES TE film (25 μm) add up to a total thickness of ~1.2 μm with a mass of 0.05 g (Extended Data Fig. 2b). The total thickness could be reduced even further if 100 μm AlN substrates were used.

TE device benchtop characterization

Benchtop characterizations of the TE devices were performed in modest vacuum (4.66 Pa (35 mTorr)), to avoid any confounding effects of room air drafts and humidity, and at room temperature of approximately 25 °C. A benchtop power supply (Xantrex XFR20-60) was used to provide constant current, and temperature was measured with a 0.0254 mm bare wire type K thermocouple mounted to a probe holder and connected to an Omega DPI32 temperature meter. Measurements and procedures were recorded manually into a laboratory notebook for every device tested. A video camera was used to record timestamps and temperature measurements during the benchtop cooling characterization for the different TE devices. We evaluated the steady-state cooling performance of the devices, because for human sensory feedback it is important for accurately conveying temperature information, such as when grasping a cold object with a prosthesis.

The ZT for each device was estimated using the Harman method by measuring the voltage across the TE module when the steady-state input current to the device is stopped^{21,52,53} (Extended Data Fig. 3c–e). We have previously used this approach and reported on the correlation between measured ZT and ΔT_{max} device performance^{21,25} (Extended Data Fig. 3f). ZT measurements from the Harman method is very effective but requires good electrical contacts to the p- and n-semiconductors, low p–n interconnect resistance, low electrical resistance of the conductive traces in the module and minimizing any mutual inductance effects in the test system. Heat transport through the wires during the Harman ZT measurement is minimized by ensuring probes are kept at heat-sink

temperatures and by letting the Peltier contact (that is, the Cu/Au/Sn interconnect with the AlN header, Extended Data Fig. 2a) thermally float.

We further minimized losses during the Harman ZT measurements by operating the TE device in a small signal mode (current (I) of 10 mA) and using a hi-gain linear amplifier with a gain of 108. Voltage values were measured using a Tektronix TBS1052B digital oscilloscope. The baseline reference voltage (or zero reference, V_{ref}) was determined from the steady-state voltage value before a steady-state input current was applied to the TE device. To measure the Peltier voltage (V_0) at time (t) equal to zero (when current is turned off) (Extended Data Fig. 3c), we used real-time boxcar averaging (Tektronix oscilloscope) of 128 continuous transient data points after the current was turned off. This averaging of the transient signal, as well as the low noise signal amplifier and ensuring minimal mutual inductance effects when the current was turned off, minimizes noise and improves signal-to-noise ratio.

The inherent TE material properties (electrical resistivity, thermal conductivity and Seebeck coefficient) of the three devices are shown in Extended Data Fig. 3g. Compared to the bulk module, the bulk_{HC} device provides 8.8 times higher a/l while having the same thermal conductivity. The CNESS thin-film device had a TE active area of 6.1 times compared to the bulk device and in fact had a lower a/l compared to the high-capacity bulk device. The TFTEC device also had lower thermal conductivity (bulk/bulk_{HC} = 0.016 W cm⁻¹ K⁻¹; thin-film, 0.008 W cm⁻¹ K⁻¹). Note that the packing fraction of the individual p–n couples within the TFTEC devices were much smaller than that of bulk modules and hence the lower active a/l for the TFTEC device. While the bulk_{HC} device had the largest aspect ratio and thermal conductance, the thin-film CNESS device had the highest ZT at the module level emanating from the improved materials (Extended Data Fig. 3g). Although ZT is not always reported at the device level, it serves as a useful metric to quantify differences across the devices and their relationship in eliciting fast and strong thermal perceptions in humans. While not reported here, we previously characterized heat-to-electric conversion efficiency and other metrics such as power density, when under a temperature gradient, using a custom device characterization set-up⁵⁴, and have shown advantages of the thin-film module²⁵.

Thermal stimulation

Thermal stimulation was provided to the surface of the skin using either a bulk TEC device (Custom Thermoelectric), a high-capacity bulk TEC device (with a special order to Custom Thermoelectric) or the thin-film TEC device described above. Both commercial TEC devices used bulk Bi₂Te₃-alloy materials. The heat collector (that is, rejection side) of every TEC device was attached to a flexible aluminium foil layer, using thermal paste (Supplementary Fig. 1) to allow for easier device placement on human skin. The bulk devices were off-the-shelf and had a total module area of 10.8 mm × 10.8 mm with a thickness of 3.5 mm. The thin-film device had a total module area of 5 mm × 6 mm and thickness of 1.2 mm.

The TEC device was connected to a power supply with constant current to achieve a target cold-side (that is, the surface touching the skin) temperature on the device. For a target temperature of 16 °C, the current supply was set to 0.4 A, 1.2 A and 1.1 A (± 0.05 A) for the bulk, bulk_{HC} and thin-film devices, respectively, with ± 0.1 A depending on the device used. The current values during thermotactile testing were set based on benchtop observations of the steady-state current needed for the desired 16 °C cold-side temperature for each device. Because it is important to convey absolute temperature for thermal sensory feedback (for example, prosthesis picks up a cold can), we evaluated TEC performance in achieving a set target temperature common across devices (that is, 16 °C). More extreme temperature targets were generally not explored due to safety considerations to avoid possible damage to the skin⁵⁵ and to remain above levels of noxious cold (<15 °C)^{56,57}. An exception is noted below during the cold-object identification experiment with participant A1.

Phantom hand sensory mapping

Thermal mapping was performed using the bulk TEC device on the residual limb of the participants with amputation. The cold-side surface, which was touching the skin, was set to a target temperature of 16 °C. The device was powered and allowed to reach the target temperature before placing on the skin. The bulk device was used for the phantom hand mapping instead of the thin-film device because the additional thickness provided by the bulk device enabled better visibility to the skin regions being contacted during thermal stimulation. Because the device was allowed to reach the target temperature (16 °C) before being placed on the skin, any of the TEC devices would have been sufficient for performing the sensory mapping.

The experimenter methodically placed the TEC device at different locations of the residual limb. Locations on the limb were probed based on known sensory mappings to the phantom hand^{15,26,27} (participants A1 and A4) in addition to other regions to identify previously unmapped sites (all participants). The participants verbally reported either not feeling the thermal sensation, feeling the sensation on the residual limb, feeling the sensation on the phantom hand or a combination of thermal sensation in both phantom and residual limb. In all cases, the thermal perception was reported as being perceived either on the residual limb or in the phantom hand.

Similar to the thermal mapping, sensory mapping of mechanical stimulation was performed on the residual limb in the same session. Using a rounded plastic probe with diameter of approximately 1 cm, the experimenter mechanically and methodically indented different locations on the residual limb of each participant. Previous sensory mappings of participants A1 and A4 were used to guide the mapping for those individuals^{15,26,27}, but all participants also underwent a full mapping of their residual limb. The participants verbally responded whether they perceived the tactile sensation on the residual limb, the phantom hand, or a combination of the two. In all cases, the mechanical stimulation sensations were perceived as being only on either the residual limb or the phantom hand and were described as being a pressure or touch.

For both thermal and mechanical sensory mapping, the participants indicated regions of perceived sensory activation in the phantom hand using a printed hand outline. This procedure of sensory mapping and marking projections to the phantom hand has been validated and used in previous studies^{5,15,26,27}.

Participants A1 and A2 returned for follow-up visits to perform the cold-object identification experiments approximately 11 months and 29 months after their initial visits, respectively. Their phantom hand sensory maps were quantified again at the beginning of their return visit.

Thermal perception experiment

For testing with participants with arm amputation, the TE device was held in place on the residual limb by the experimenter, or, if possible, the TE device was set on a table and the participant rested their residual limb on the device. At least two stimulation sites were used to provide thermal sensations: one that elicited thermal sensations on the residual limb itself and one that elicited sensations in the phantom hand. For non-amputee participants, the TE device was set on a flat surface, and the participants placed the tip of their index finger on their dominant hand on the cold-side surface of the device. A microcontroller (Arduino Micro) was used to monitor safe temperature levels and record voltage input to the TE device (Supplementary Fig. 1a). Voltage data were sampled at 200 Hz. TE voltage levels were monitored to record when stimulation was being applied and the time delay between onset of thermal stimulation and participant reaction. Using a custom graphical user interface, built in MATLAB, the participant pressed a keyboard button as soon as a change in thermal sensation was detected (Supplementary Fig. 1b). A visual cue was displayed to indicate when the thermal stimulation

trial began. The participants with arm amputation used their opposing arm to press the keyboard. The non-amputee participants used their non-dominant hand to respond. Reaction time was measured as the time delay between thermal stimulus onset and the key press after a change in thermal perception was detected by the participant. Using a sliding scale in the graphical user interface, the participant reported their subjective perception of the thermal intensity for each trial. The thermal stimulation lasted up to 10 s, and stimulation was turned off as soon as the participant reported a perceived change in temperature.

The participants were instructed to press the keyboard button whenever they perceived a change in temperature in their skin or their phantom limb. The participants were not told whether they would receive cooling, warming or nothing; rather, they were instructed to respond to any change in thermal sensation and then report whether it was cooling, warming or nothing.

All amputee participants performed the experiment with both the standard bulk and the thin-film TEC devices. Participant A4 also performed the experiment with the bulk_{HC} device (Extended Data Fig. 6). All of the non-amputee participants performed the experiment with both the standard bulk and the thin-film TEC devices. Two of the non-amputee participants also performed the experiment with the bulk_{HC} device (Extended Data Fig. 7).

For each device, thermal stimulation was performed at least 10 times at each site for the participants with amputation and at least 20 times for the non-amputee participants. Blocks of five trials were conducted, and the device used in each block was randomized to avoid desensitization and bias. The participants could physically see which device was being used. A break between 30 s and 60 s was allowed between each trial for the thermal sensation to subside in the skin and to allow the TE device to return to a steady state at room temperature. A break of up to 5 min was allowed between each block of trials. A target cold-side surface temperature of 16 °C was used for all devices, and each trial started at approximately room temperature (~22–25 °C). The target temperature was used to measure the ability of each device, when being driven to a particular steady-state value, in eliciting thermal sensations, which is important for providing real-time sensory feedback to humans.

Participant A1 also performed the experiment with a target cooling temperature of 23 °C, starting from approximately 25 °C. These results are reported separately in Extended Data Fig. 6a, but these trials were used when calculating the probability of thermal detection of the different devices (Fig. 3b).

Participant A4 reported sensations of warming on some trials and cooling on others. A change in thermal sensation was detected by the participant on every trial, so we combined these results in Fig. 3 but show them separately in Extended Data Fig. 6. The other participants reported sensations of cooling on every trial.

Thermal perception repeatability experiment

One of the non-amputee participants (B2, male, 30 years old at study onset) performed the perception repeatability study with the TFTEC device. This experiment was the same as the thermal perception experiment but was conducted over a continuous period of 180 min. The device was strapped to the index fingertip on the non-dominant hand and secured in place using medical tape. Attaching the device did not impede fingertip movements. The participant used the dominant hand to press the keyboard whenever they perceived thermal sensation on the index finger and reported the perceived intensity of the sensation after each trial. Three thermal stimulation trials were provided in each block, and blocks were separated by a random delay of 7–15 min. The participant performed 15 blocks over 180 min. The target cold-side surface temperature was set to 16 °C for every trial. There was no special skin preparation or TFTEC device packaging optimization for this experiment.

Baseline visual-reaction experiment

Baseline reaction to visual stimuli was measured using the same user interface as the thermal perception experiment. The participants pressed a button on the keyboard as soon as they saw a visual cue on the screen. Amputee participants A2–A4 performed one block (30 trials), and non-amputee participants B1–B4 performed two blocks (60 trials, B2, B4) or three blocks (90 trials, B1, B3).

Cold-object detection experiment

To demonstrate real-world functional benefit of thermal sensory feedback to an individual with arm amputation, we designed an experiment in which three visually identical beverage cans were placed on a table and the participant was asked to identify the cold can within a given amount of time. The cans were aluminium and were approximately 12.2 cm in height with a diameter of 6.6 cm and held a volume of 355 ml. One of the objects (that is, cans) was cooled to approximately 5–15 °C, using a refrigerator, while the other objects were kept at ambient temperature (20–25 °C, mean: 22.8 °C).

To perform the experiment, participant A1 used the MPL, an advanced prosthesis with up to 26 articulating joints developed at the Johns Hopkins University Applied Physics Laboratory and used in numerous prosthesis and brain–computer interface-related studies^{50,58,59}. The MPL was controlled using the Virtual Integration Environment, and an infrared temperature sensor (MLX90615, Melexis) was embedded in a custom 3D printed fingertip on the prosthesis. The temperature sensor was calibrated after integration into the MPL fingertip, and temperature measurements were corrected using a linear scaling factor. The infrared temperature sensor was connected to a Bluetooth-enabled microcontroller (Feather 32u4 Bluefruit LE, Adafruit) and lithium-ion battery, which were mounted to the back of the MPL hand. Temperature sensor signals were transmitted to a laptop at approximately 10 Hz.

A custom hardware interface was used to connect the MPL to the participant's osseointegrated abutment^{33,50}, and a wireless electromyography (EMG) armband (Myo, Thalmic Labs) was used to stream EMG signals over Bluetooth at 200 Hz to an onboard controller in the prosthesis^{50,60}. The EMG armband had eight stainless steel electrode pairs, which were uniformly distributed around the participant's residual limb (Fig. 5).

Real-time EMG movement decoding was performed using a linear discriminant analysis classifier, which was implemented on the onboard controller in the MPL. Time domain features (mean absolute value, waveform length, slope sign change and zero crossings⁶¹) were extracted from the EMG signal using a 250 ms sliding window with a 20 ms step size. Training data for each desired movement (for example, elbow flexion, hand open and so on) were collected using a mobile interface to the onboard controller in the MPL. The participant had extensive EMG pattern recognition experience⁵⁰ and collected several seconds of training data for each movement. For the experiment, the participant trained the pattern recognition algorithm to decode elbow extension, elbow flexion, hand close, hand open and no movement (that is, 'rest'). Offline classification accuracy, which was calculated using a leave-one-out training and testing strategy with each training data set being separated into five segments, is shown in Extended Data Fig. 8.

The thin-film TEC device was attached to a stimulation site on the participant's residual limb that elicited sensations in the phantom fingers (Fig. 5a and Extended Data Fig. 1). The participant noted that towards the end of the testing session on each day he began to also perceive thermal sensations on the residual limb, at the site of stimulation; however, thermal activation of the fingers was still perceived. On the first day of this experiment, the infrared temperature sensor was placed on the little finger of the MPL so that it would correspond with thermal sensation in the little finger of the phantom hand. On the second day, the ring finger of the phantom hand was noted as being stronger during

thermal stimulation, so the infrared temperature sensor was moved to the ring finger on the MPL.

Thermal stimulation was delivered to the participant when the infrared temperature sensor in the prosthesis was below approximately 14 °C. Because the cold object's temperature was within a range of 5–15 °C and to ensure consistency across trials as the cold object would inevitably warm up slightly, the thermal stimulation cold-side target was set to 10 °C ($I_{\text{bulk}} = 1.0 \text{ A}$, $I_{\text{bulkHC}} = 2.1 \text{ A}$, $I_{\text{thin-film}} = 2.1 \text{ A}$). Because the cold-side target was below the threshold for noxious cold^{56,57}, we confirmed with the participant that he did not perceive any painful or uncomfortable sensations as a result of the thermal stimulation. We also visually inspected the stimulation site periodically to ensure skin damage was not occurring due to excessive cooling.

Each trial consisted of the experimenter placing the objects in a row on a table in front of the participant. The cold object was randomly placed in one of the three locations (that is, left, centre or right). The participant was given up to 90 s for each trial and instructed to find the cold can using only the prosthesis to feel each one. The participant verbally indicated which object was the cold one. In between trials, the experimenter wiped off the cold object after each trial to remove any condensation or other visual indications of temperature. As the cold object would warm up because of being in ambient conditions, it was regularly replaced with another cold object. Trials were conducted in blocks of five and were carried out over a 2 day period for a total of 19 trials. The participant was allowed to practice with room temperature objects (without thermal stimulation) for up to 5 min before the experiment began.

Trials were controlled using a custom MATLAB script that audibly indicated trial start and end as well as recorded sensor signals and participant responses. A Canon VIXIA HF G20 camera and a Jenoptik VairoCAM HD thermography camera were used to record video footage of the trials.

Finally, to ensure that the participant was not using visual cues to identify the cold object, we measured baseline performance where the participant guessed which object was cold using only visual information (Fig. 5c). The participant's chance performance was 30% (6/20 trials).

Virtual cold-object detection experiment

Similar to the cold-object identification experiment using the physical prosthesis, we developed a virtual version of the same task to enable additional data collection across more participants and TEC devices. The vMPL, which is a virtual version of the MPL and operates using the same Virtual Integration Environment software architecture as the physical limb^{60,62,63}, was controlled by participants to 'feel' virtual objects (Extended Data Fig. 8).

Two amputee participants (A1 and A2, 2 males, 41–65 years old at study onset) and two non-amputee participants (B5 and B6, 1 male, 1 female, 22–26 years old at study onset) performed the experiment. Thermal stimulation was mapped to the index, middle, and ring finger for A1 (Extended Data Fig. 1c). Thermal stimulation was delivered to the tip of the ring finger for A2 (Extended Data Fig. 1b) and to the tip of the index finger for the non-amputee participants (Extended Data Fig. 8d). One of the three virtual objects was 'cold' and, when touched by the corresponding vMPL finger(s), triggered thermal stimulation to the participant. The cold-side target temperature for each TEC device was set to 16 °C for all participants, except for A1 in which case the target was set to 10 °C to match the thermal stimulation used in the physical cold-object detection experiment.

The virtual cold object was randomly assigned to one of the three objects, and participants were given up to 45 s to complete each trial. Participants were instructed to identify the cold object as fast as they could on each trial.

The vMPL was controlled using the Myo armband. Participant A1 used EMG pattern recognition control to perform elbow flexion and extension movements. For all other participants, two Myo armbands

were worn: one on the upper arm and one below the elbow. Arm orientation was tracked using embedded inertial measurement units (IMUs) in each armband, transformed and mapped to vMPL movements. IMU signals were streamed wirelessly to a laptop at approximately 50 Hz. No EMG movement decoding was used to control the vMPL, with the exception of the trials performed with A1.

The objects were oriented on the horizontal plane, similar to the physical version of the task, in front of the vMPL for all participants (Extended Data Fig. 8a) except for A1. Because participant A1 has a transhumeral amputation, he was unable to use the IMU forearm motion tracking with elbow movements for the virtual experiment. Instead, the virtual objects were oriented vertically, and the participant used EMG signals to control elbow flexion and extension to position the vMPL and touch each virtual object. Virtual objects were positioned such that every participant could easily control the vMPL to make contact with each one.

Trials were conducted in blocks of five with a target of at least 10 trials total for each TEC device on each participant. The TEC device order was randomized in each block for the non-amputee participants. Device ordering was not effectively randomized for the amputee participants due to lack of time. However, results from both participant groups are similar, suggesting that learning effects likely did not play a role in this experiment.

Participant A2 performed the study only using the high-capacity bulk (I_{bulk}) and thin-film TEC devices. The other participants used bulk, I_{bulkHC} and thin-film TEC devices. The participants performed the experiment in one session, with the exception of A1 who performed the experiments on both days of his follow-up visit.

Trials were controlled using a custom MATLAB script to begin and end trials while also recording vMPL movements and interactions in the virtual environment.

Data analysis

For each participant, reaction times and reported intensity levels from successful thermal detection trials at each target temperature were averaged together. Trials where thermal changes were not perceived within the trial duration were not included in calculating the average response time or reported intensity. Perceived intensity results were scaled from 0 to 10, with 10 being the maximum possible response on the graphical sliding scale. Normalized reaction time to thermal stimulation was achieved by subtracting the mean visual reaction time from the thermal reaction time data for each participant. Because A1 did not perform the reaction time experiment, the actual reaction to thermal stimulation was reported when combining amputee data (Fig. 3c). Combining perceived intensity across participants was done by rescaling such that the maximum reported intensity from each participant was a '10'.

Results from the amputee participants were not combined with the results from the non-amputee participants. Results from thermal stimulation on the phantom limb were not combined across participants given that each amputation and region of stimulation is unique to each individual.

The time spent touching each object in the virtual cold-object detection experiment was calculated as the total time the vMPL was contacting a virtual object with the target finger(s) (for example, index, middle and ring fingers for A1, ring finger for A2, and index finger for non-amputee participants) before moving to the next object. Contact times of less than 750 ms were removed to avoid accidental touches by passing through objects during vMPL control. Time touching each object from the non-amputee participants were combined after using max–min normalization for each participant using equation (3):

$$T = \frac{T - \min(T)}{\max(T) - \min(T)} \quad (3)$$

where T is the time touching objects across all TEC devices for an individual participant and T' is the feature scaled result, resulting in a normalized range of [0 to 1].

Statistical P values were calculated using a two-sided Mann–Whitney U -test. Data from the thermal perception experiments were not assumed to be normally distributed (Shapiro–Wilk test⁶⁴, $P < 0.05$). Statistical comparisons between groups were made only if there were at least three data points within one of the groups. Bar plots represent the mean, and error bars represent the standard error of the mean, unless otherwise specified. Where trend lines are shown, a linear regression model was fit to the data using ordinary least squares. A one-sample t -test was used to calculate the statistical P values for the regression line slopes. Human data analysis was performed using MATLAB (MathWorks), and benchtop TEC device data analysis was performed using Excel (Microsoft). Thermogram image analysis was performed using IRBIS 3 Professional (InfraTec). Supplementary videos were prepared using Premiere Pro (Adobe).

Reporting summary

Further information on research design is available in the Nature Portfolio Reporting Summary linked to this article.

Data availability

All source data generated or analysed during the study and needed to interpret and verify the findings are available within the paper and its Supplementary Information. Source data are provided with this paper.

Code availability

The code used for controlling the virtual and physical prosthetic limb is available at <https://bitbucket.org/rarmiger/minivie>. The custom Arduino code used for monitoring and controlling thermal stimulation and the custom MATLAB code used for running the thermal-reaction-time experiment and for analysing the data are available for research purposes from the corresponding authors on reasonable request.

References

1. Abaira, V. E. & Ginty, D. D. The sensory neurons of touch. *Neuron* **79**, 618–639 (2013).
2. Schepers, R. J. & Ringkamp, M. Thermoreceptors and thermosensitive afferents. *Neurosci. Biobehav. Rev.* **34**, 177–184 (2010).
3. Graczyk, E. L. et al. The neural basis of perceived intensity in natural and artificial touch. *Sci. Transl. Med.* **8**, 362ra142 (2016).
4. Oddo, C. M. et al. Intraneural stimulation elicits discrimination of textural features by artificial fingertip in intact and amputee humans. *eLife* **5**, e09148 (2016).
5. Osborn, L. E. et al. Prosthesis with neuromorphic multilayered e-dermis perceives touch and pain. *Sci. Robot.* **3**, eaat3818 (2018).
6. Kuiken, T. A., Marasco, P. D., Lock, B. A., Harden, R. N. & Dewald, J. P. A. Redirection of cutaneous sensation from the hand to the chest skin of human amputees with targeted reinnervation. *Proc. Natl Acad. Sci. USA* **104**, 20061–20066 (2007).
7. Ortiz-Catalan, M., Mastinu, E., Sassu, P., Aszmann, O. & Brånemark, R. Self-contained neuromusculoskeletal arm prostheses. *N. Engl. J. Med.* **382**, 1732–1738 (2020).
8. Srinivasan, S. S. & Herr, H. M. A cutaneous mechanoneural interface for neuroprosthetic feedback. *Nat. Biomed. Eng.* **6**, 731–740 (2022).
9. Bensmaïa, S. J., Tyler, D. J. & Micera, S. Restoration of sensory information via bionic hands. *Nat. Biomed. Eng.* **7**, 443–455 (2023).
10. Raspopovic, S., Valle, G. & Petrini, F. M. Sensory feedback for limb prostheses in amputees. *Nat. Mater.* **20**, 925–939 (2021).
11. Bohic, M. & Abaira, V. E. Wired for social touch: the sense that binds us to others. *Curr. Opin. Behav. Sci.* **43**, 207–215 (2022).
12. Zbinden, J., Lendaro, E. & Ortiz-Catalan, M. A multi-dimensional framework for prosthetic embodiment: a perspective for translational research. *J. Neuroeng. Rehabil.* **19**, 122 (2022).
13. Srinivasan, S. S. et al. On prosthetic control: a regenerative agonist–antagonist myoneural interface. *Sci. Robot.* **2**, eaan2971 (2017).
14. Valle, G. et al. Biomimetic intraneural sensory feedback enhances sensation naturalness, tactile sensitivity, and manual dexterity in a bidirectional prosthesis. *Neuron* **100**, 37–45 (2018).
15. Osborn, L. E. et al. Sensory stimulation enhances phantom limb perception and movement decoding. *J. Neural Eng.* **17**, 056006 (2020).
16. Christie, B. P. et al. Ambulatory searching task reveals importance of somatosensation for lower-limb amputees. *Sci. Rep.* **10**, 1–11 (2020).
17. George, J. A. et al. Biomimetic sensory feedback through peripheral nerve stimulation improves dexterous use of a bionic hand. *Sci. Robot.* **4**, eaax2352 (2019).
18. Preatoni, G., Valle, G., Petrini, F. M. & Raspopovic, S. Lightening the perceived prosthesis weight with neural embodiment promoted by sensory feedback. *Curr. Biol.* **31**, 1065–1071 (2021).
19. Graczyk, E. L., Resnik, L., Schiefer, M. A., Schmitt, M. S. & Tyler, D. J. Home use of a neural-connected sensory prosthesis provides the functional and psychosocial experience of having a hand again. *Sci. Rep.* **8**, 9866 (2018).
20. Merrill, D. R., Bikson, M. & Jefferys, J. G. R. Electrical stimulation of excitable tissue: design of efficacious and safe protocols. *J. Neurosci. Methods* **141**, 171–198 (2005).
21. Venkatasubramanian, R., Siivola, E., Colpitts, T. & O’Quinn, B. Thin-film thermoelectric devices with high room-temperature figures of merit. *Nature* **413**, 597–602 (2001).
22. Jin, Q. et al. Flexible layer-structured Bi₂Te₃ thermoelectric on a carbon nanotube scaffold. *Nat. Mater.* **18**, 62–68 (2019).
23. Sun, T. et al. Stretchable fabric generates electric power from woven thermoelectric fibers. *Nat. Commun.* **11**, 1–10 (2020).
24. Venkatasubramanian, R., Pierce, J. M. & Dezsi, G. Superlattice structures for thermoelectric devices. US patent 10,903,139 (2021).
25. Venkatasubramanian, R., Pierce, J. M., Himmtann, M., Dezsi, G. & Rhim, Y.-R. Thin-film thermoelectric conversion devices for direct thermal-to-electric conversion for DC and pulse power. *Johns Hopkins APL Tech. Dig.* **35**, 448–452 (2021).
26. Osborn, L. et al. Phantom hand activation during physical touch and targeted transcutaneous electrical nerve stimulation. In *MEC Symposium Conference* (2020).
27. Osborn, L. et al. Targeted transcutaneous electrical nerve stimulation for phantom limb sensory feedback. In *IEEE Trans. Biomed. Circuits Syst.* 1–4 (2017); <https://doi.org/10.1109/BIOCAS.2017.8325200>
28. Luo, M. et al. High-density thermal sensitivity maps of the human body. *Build. Environ.* **167**, 106435 (2020).
29. Green, B. G. & Akirav, C. Threshold and rate sensitivity of low-threshold thermal nociception. *Eur. J. Neurosci.* **31**, 1637–1645 (2010).
30. Adair, R. K. A model of the detection of warmth and cold by cutaneous sensors through effects on voltage-gated membrane channels. *Proc. Natl Acad. Sci. USA* **96**, 11825–11829 (1999).
31. Chowdhury, I. et al. On-chip cooling by superlattice-based thin-film thermoelectrics. *Nat. Nanotechnol.* **4**, 235–238 (2009).
32. Venkatasubramanian, R., Osborn, L. E., Armiger, R. S., Himmtann, M. & Pierce, J. M. Fast-rate thermoelectric device. US patent 11,227,988 (2022).

33. Johannes, M. S. et al. In *Wearable Robotics* (eds Rosen, J. & Ferguson, P. W.) 393–444 (Academic, 2020).
34. Izawa, J. & Shadmehr, R. On-line processing of uncertain information in visuomotor control. *J. Neurosci.* **28**, 11360–11368 (2008).
35. Wei, K. & Koerding, K. Uncertainty of feedback and state estimation determines the speed of motor adaptation. *Front. Comput. Neurosci.* **4**, 11 (2010).
36. Zhu, K., Perrault, S., Chen, T., Cai, S. & Lalintha Peiris, R. A sense of ice and fire: exploring thermal feedback with multiple thermoelectric-cooling elements on a smart ring. *Int. J. Hum. Comput. Stud.* **130**, 234–247 (2019).
37. Gallo, S. et al. Encoded and crossmodal thermal stimulation through a fingertip-sized haptic display. *Front. Robot. AI* **2**, 25 (2015).
38. Kim, S. et al. Two-dimensional thermal haptic module based on a flexible thermoelectric device. *Soft Robot.* **7**, 736–742 (2020).
39. Kishore, R. A., Nozariabmarz, A., Poudel, B., Sanghadasa, M. & Priya, S. Ultra-high performance wearable thermoelectric coolers with less materials. *Nat. Commun.* **10**, 1765 (2019).
40. Lee, J. et al. Stretchable skin-like cooling/heating device for reconstruction of artificial thermal sensation in virtual reality. *Adv. Funct. Mater.* **30**, 1909171 (2020).
41. Chatt, A. B. & Kenshalo, D. R. Cerebral evoked responses to skin warming recorded from human scalp. *Exp. Brain Res* **28**, 449–455 (1977).
42. Li, G. et al. Integrated microthermoelectric coolers with rapid response time and high device reliability. *Nat. Electron.* **1**, 555–561 (2018).
43. Ren, W. et al. High-performance wearable thermoelectric generator with self-healing, recycling, and Lego-like reconfiguring capabilities. *Sci. Adv.* **7**, eabe0586 (2021).
44. Dunham, M. T. et al. Experimental characterization of microfabricated thermoelectric energy harvesters for smart sensor and wearable applications. *Adv. Mater. Technol.* **3**, 1700383 (2018).
45. Kim, F. et al. 3D printing of shape-conformable thermoelectric materials using all-inorganic Bi₂Te₃-based inks. *Nat. Energy* **3**, 301–309 (2018).
46. Jo, S., Choo, S., Kim, F., Heo, S. H. & Son, J. S. Ink processing for thermoelectric materials and power-generating devices. *Adv. Mater.* **31**, 1804930 (2019).
47. Beukema, P. et al. TrpM8-mediated somatosensation in mouse neocortex. *J. Comp. Neurol.* **526**, 1444–1456 (2018).
48. Naver, H. et al. Autonomic and thermal sensory symptoms and dysfunction after stroke. *Stroke* **26**, 1379–1385 (1995).
49. Xue, M. & Jackson, C. J. Extracellular matrix reorganization during wound healing and its impact on abnormal scarring. *Adv. Wound Care* **4**, 119–136 (2015).
50. Osborn, L. E. et al. Extended home use of an advanced osseointegrated prosthetic arm improves function, performance, and control efficiency. *J. Neural Eng.* **18**, 026020 (2021).
51. Hebert, J. S. et al. Novel targeted sensory reinnervation technique to restore functional hand sensation after transhumeral amputation. *IEEE Trans. Neural Syst. Rehabil. Eng.* **22**, 765–773 (2014).
52. Roh, I. J. et al. Harman measurements for thermoelectric materials and modules under non-adiabatic conditions. *Sci. Rep.* **6**, 1–10 (2016).
53. Harman, T. C. Special techniques for measurement of thermoelectric properties. *J. Appl. Phys.* **29**, 1373–1374 (1958).
54. Cook, B. A. et al. High-performance three-stage cascade thermoelectric devices with 20% efficiency. *J. Electron. Mater.* **44**, 1936–1942 (2015).
55. Geng, Q. et al. Temperature limit values for touching cold surfaces with the fingertip. *Ann. Occup. Hyg.* **50**, 851–862 (2006).
56. McKemy, D. D. The molecular and cellular basis of cold sensation. *ACS Chem. Neurosci.* **4**, 238–247 (2012).
57. Simone, D. A. & Kajander, K. C. Responses of cutaneous A-fiber nociceptors to noxious cold. *J. Neurophysiol.* **77**, 2049–2060 (1997).
58. Osborn, L. E. et al. Monitoring at-home prosthesis control improvements through real-time data logging. *J. Neural Eng.* **19**, 036021 (2022).
59. Handelman, D. A. et al. Shared control of bimanual robotic limbs with a brain-machine interface for self-feeding. *Front. Neurobot.* **16**, 918001 (2022).
60. Perry, B. N. et al. Virtual integration environment as an advanced prosthetic limb training platform. *Front. Neurol.* **9**, 785 (2018).
61. Englehart, K. & Hudgins, B. A robust, real-time control scheme for multifunction myoelectric control. *IEEE Trans. Biomed. Eng.* **50**, 848–854 (2003).
62. Armiger, R. S. et al. A real-time virtual integration environment. *Johns Hopkins APL Tech. Dig.* **30**, 198–206 (2011).
63. Wester, B. A. et al. CONVEY: connecting STEM outreach now using VIE education for youth. *Johns Hopkins APL Tech. Dig.* **35**, 259–266 (2020).
64. Shapiro, S. S. & Wilk, M. B. An analysis of variance test for normality (complete samples). *Biometrika* **52**, 591–611 (1965).
65. Goldsmid, H. J. In *CRC Handbook of Thermoelectrics* (ed. Rowe, D. M.) 19–26 (CRC, 1995).
66. Semenyuk, V. In *Thermoelectrics Handbook* (ed. Rowe, D. M.) 58-1-58-21 (Taylor & Francis, 2006).
67. von Gunten, K. Thermal cyler optimized for real-time DNA analysis. *EE Times* (2012).

Acknowledgements

The authors thank the participants who contributed their time to improving the technology for those with upper-extremity impairment. The authors thank B. Christie for reviewing results and analysis, M. Iskarous for assistance with managing ethical-approval documentation, J. Forsberg and P. Pasquina for programmatic support, B. Wester for data-visualization guidance and C. Carneal for programmatic guidance and support. R.S.A. acknowledges support from the Uniformed Services University of Health Sciences and the Henry M. Jackson Foundation for the Advancement of Military Medicine (HJF) under federal awards HU00011520028 and HU00012020062. L.E.O. acknowledges internal research support from the Johns Hopkins University Applied Physics Laboratory. R.V. acknowledges support for the original development of CHES thin-film thermoelectric materials and technology from the Defense Advanced Research Projects Agency (DARPA) under contract HRO011-16-C-0011. The MPL and vMPL were previously developed as part of the DARPA Revolutionizing Prosthetics Program. The views expressed in this article are those of the authors and do not reflect the official policy of HJF, the Department of Army/Navy/Air Force, Department of Defense or the US Government. The opinions and assertions expressed herein are those of the authors and do not necessarily reflect the official policy or position of the Uniformed Services University or the Department of Defense.

Author contributions

L.E.O., R.V., M.H., A.C.G.C., C.W.M., J.M.W., H.H.N., M.S.F. and R.S.A. designed, implemented and conducted the thermotactile experiments. R.V., M.H., P.G. and R.J.U. designed, fabricated and tested the TFTEC devices and their integration into suitable heat sinks for human participant testing. J.M.P. performed epitaxial thin-film growth needed for the TFTEC devices. L.E.O. performed data visualization. L.E.O. and R.V. wrote the manuscript. All authors contributed to editing and reviewing the manuscript.

Competing interests

R.V., L.E.O., M.H., J.M.P. and R.S.A. are inventors on intellectual property pertaining to thin-film thermoelectric devices and US patents 11,227,988 and 11,532,778 and application 18/071,789. R.V. and J.M.P. are inventors on US patent 10,903,139. The Johns Hopkins University is the applicant on these patents. The other authors declare no competing interests.

Additional information

Extended data is available for this paper at <https://doi.org/10.1038/s41551-023-01070-w>.

Supplementary information The online version contains supplementary material available at <https://doi.org/10.1038/s41551-023-01070-w>.

Correspondence and requests for materials should be addressed to Luke E. Osborn or Rama Venkatasubramanian.

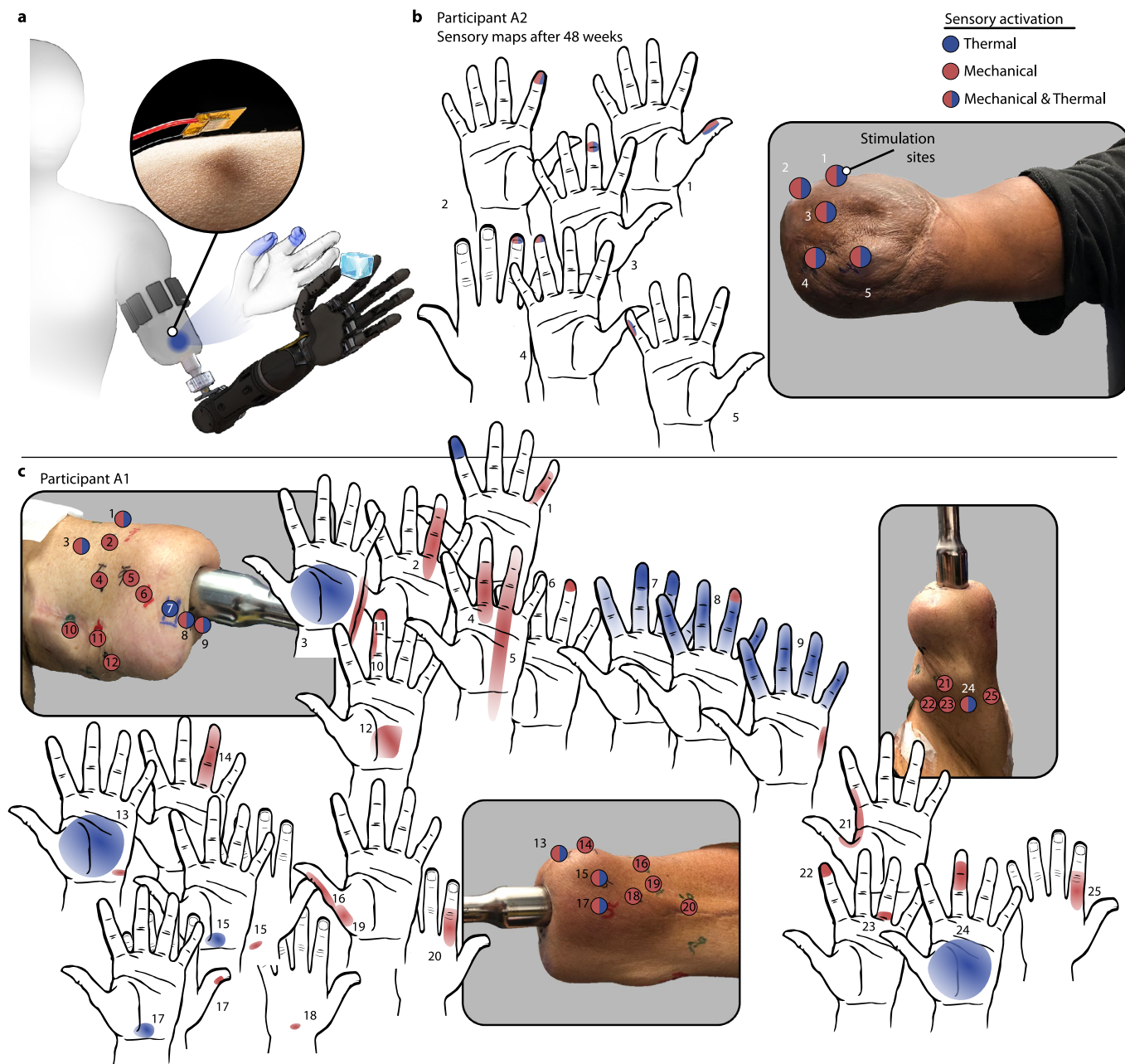
Peer review information *Nature Biomedical Engineering* thanks Kornelius Nielsch and the other, anonymous, reviewer(s) for their contribution to the peer review of this work. Peer reviewer reports are available.

Reprints and permissions information is available at www.nature.com/reprints.

Publisher's note Springer Nature remains neutral with regard to jurisdictional claims in published maps and institutional affiliations.

Springer Nature or its licensor (e.g. a society or other partner) holds exclusive rights to this article under a publishing agreement with the author(s) or other rightsholder(s); author self-archiving of the accepted manuscript version of this article is solely governed by the terms of such publishing agreement and applicable law.

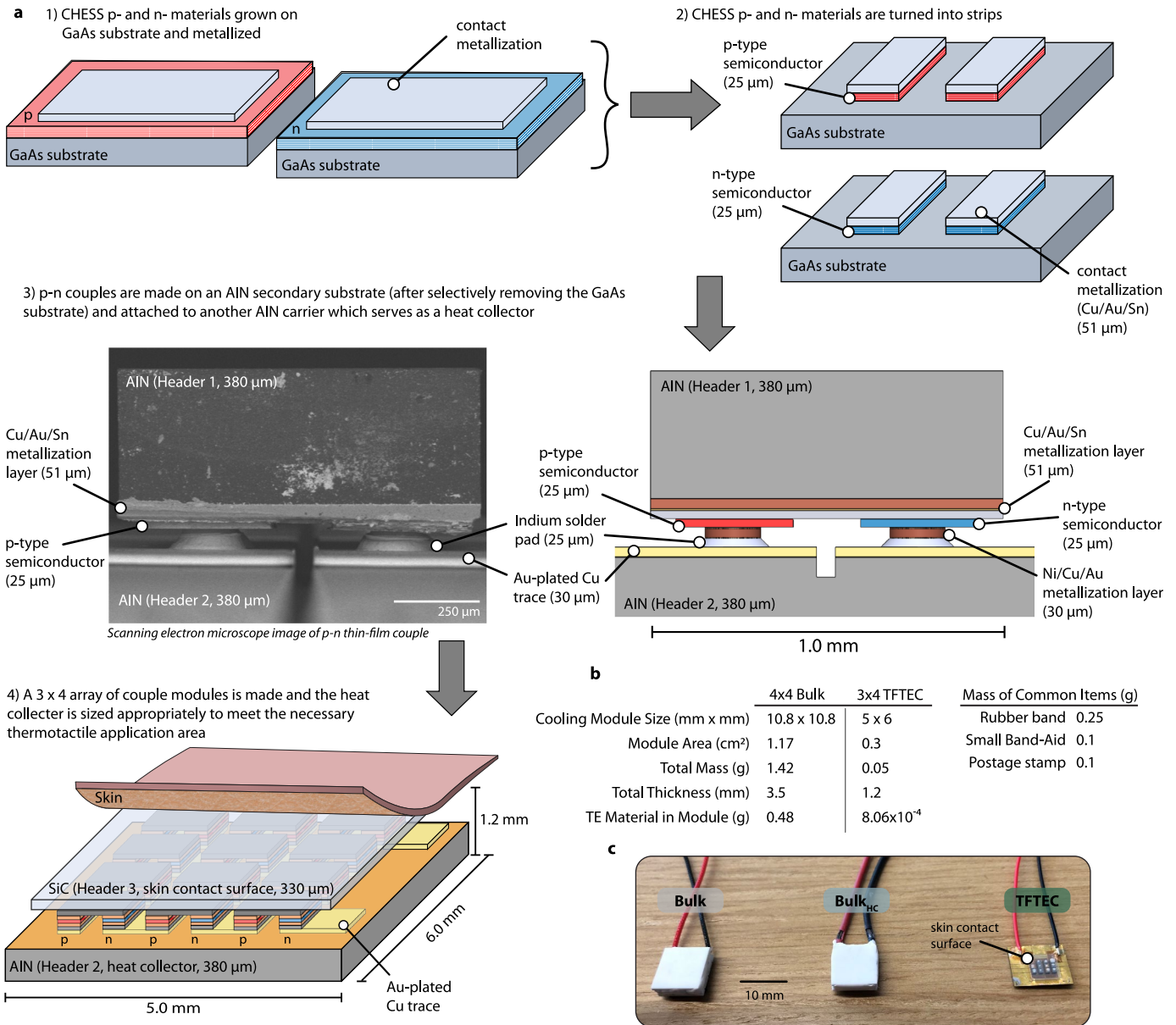
© The Author(s), under exclusive licence to Springer Nature Limited 2023



Extended Data Fig. 1 | Thermal sensations are stable over 11 months.

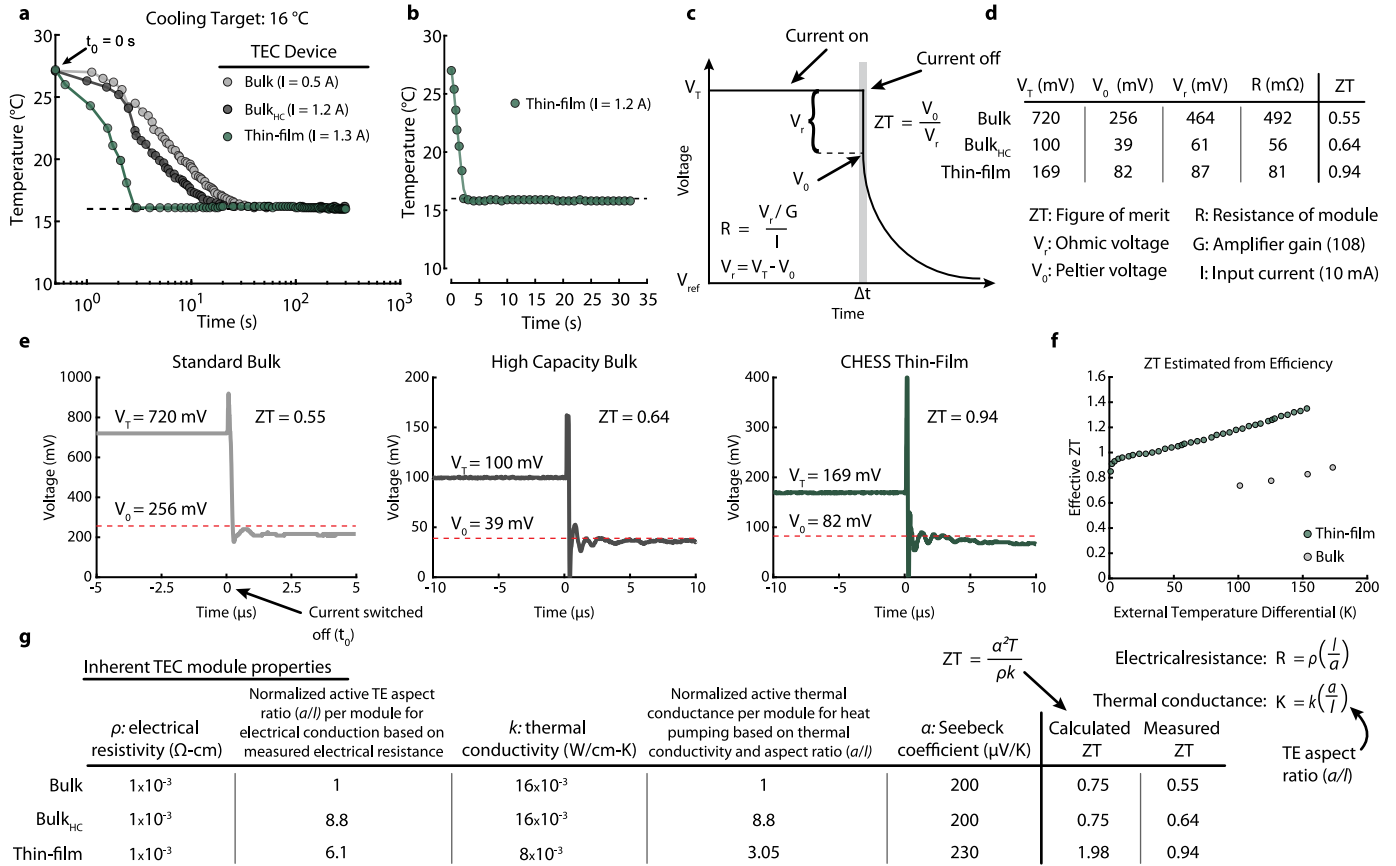
a, Noninvasive thermal stimulation of the skin was used to restore thermal sensations in the phantom hand using thin-film thermoelectric cooling (TFTEC) devices and enable perception of cold objects during grasping with a prosthesis. **b**, The activated regions of the phantom hand remained similar after 11 months (48 weeks) for participant A2, showing long-term stability of restored thermal perceptions. This stability aligns with previously documented stability in phantom hand sensory maps for other stimulation modalities¹⁵. **c**, Participant

A1 underwent an unrelated surgery on the amputated arm after the initial sensory mapping, which affected the phantom hand sensory maps. Sensory sites were mapped again 29 months (128 weeks) after the initial mapping session. Although activated regions changed due to the unrelated surgery, we were able to convey thermal sensations to the phantom hand. With the new sensory sites, we observed similarities from previous sites in that mechanical and thermal perceptions did not always project to the same region of the phantom hand despite the same site of stimulation.



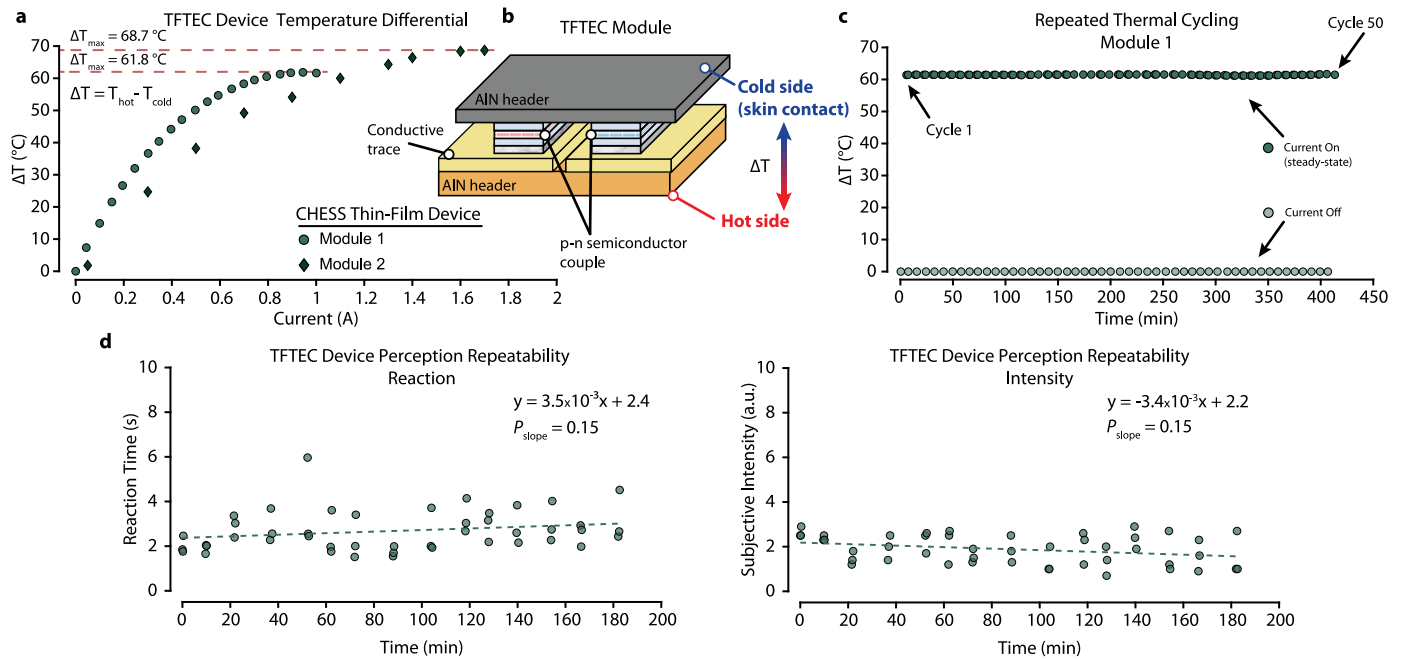
Extended Data Fig. 2 | TFTEC device fabrication. **a**, Key steps in the fabrication of a TFTEC module, used in this study, utilizing the Controlled Hierarchically Engineered Superlattice Structures (CHES) materials. 1) 25 μm p-type and n-type CHES thin-films are grown on GaAs substrates and a metallization layer (Cu/Au/Sn, 51 μm) is placed on top of the thin-films. 2) The p-type and n-type materials are cut into strips and 3) are bonded onto an AlN substrate (Header 1, 380 μm). An additional metallization layer (Ni/Cu/Au, 30 μm) is placed, which is used to bond the CHES thin-films onto Au-plated Cu traces (30 μm) with an In alloy solder (25 μm) to form a single p-n couple module. 4) A 3 × 4 array of the p-n coupled modules is assembled on a common AlN substrate (Header 2, 380 μm), which acts as a heat collector, and an additional SiC common header (Header 3, 330 μm) is placed on top of the module array, connecting the p-n couples in

parallel and enabling contact with the skin. **b**, Physical dimensions of the thin-film thermoelectric cooling (TFTEC) and bulk devices, showing the benefits of the TFTEC for wearable applications. The total mass of the TFTEC module is about 1/2 of a small Band-Aid or 1/5th of a rubber band. It is worth noting that the TFTEC module is 1/28th the total mass of the bulk module, and uses ~1/600th the active TE material mass for better functionality. Future development of TFTEC devices can include lowering the weight of AlN (Headers 1, 2, and 3) enabling more lightweight thermotactile packages, while keeping the functionality of cooling and heating. The TFTEC technology for thermotactile applications presented here is a proof-of-concept demonstration in producing biologically relevant speeds of cooling. **c**, The three types of thermoelectric cooling device used in the thermotactile experiments.



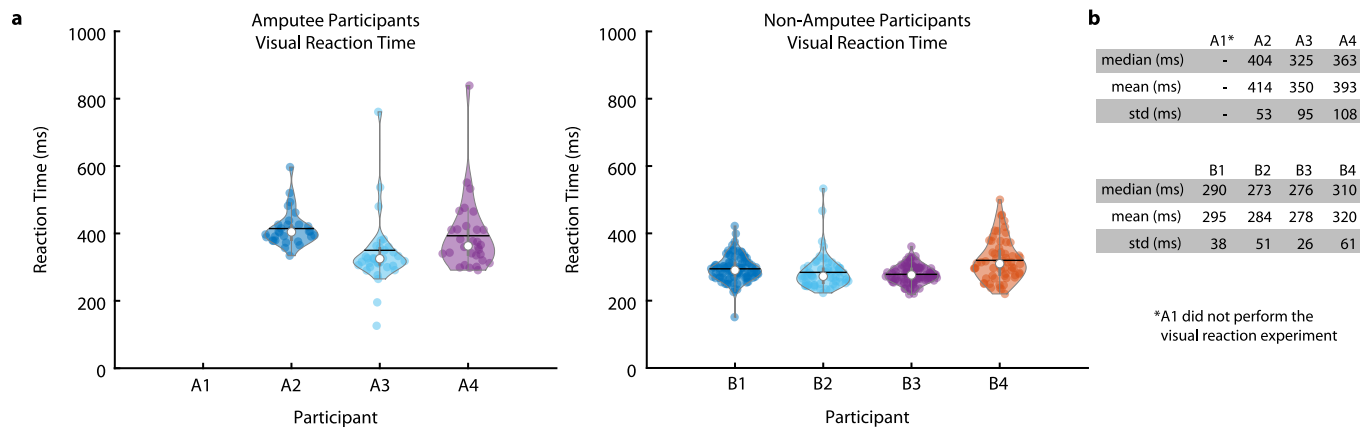
Extended Data Fig. 3 | Steady-state thermoelectric device cooling response, material properties, and figures of merit. a, All three of the TEC devices remained stable and did not deviate once reaching the target temperature value. Differences in current used, compared to Fig. 2g, is because the input current to reach a target temperature can vary ±0.1 A across modules. **b**, Steady-state response of the thin-film module used with participant A1 for the cold object identification experiments. **c**, The figure of merit (ZT) was estimated using the Harman method to measure Ohmic (V_r) and Peltier (V_o) voltage components when TEC device input current was switched off. **d**, Measured voltage values for each TEC device used to estimate the ZT. e, V_T was estimated as the voltage at steady state before current was switched off (t₀) and V_o was estimated by the voltage immediately after input current is removed. Measurements were taken at T = 300 K. **f**, Effective ZT estimated from thermal efficiency for thin-film (1 × 4

array) and bulk thermoelectric generator (TEG) devices. Data redrawn with permission from²⁵. **g**, Inherent material properties of both p- and n-type materials were nominally the same in TFTEC modules and generally the same approach of comparable p- and n-type material properties are used by manufacturers of bulk modules⁶⁵. Despite having a smaller active aspect ratio compared to bulk_{HC}, the thin-film device has larger ZT and a slightly higher Seebeck coefficient, which leads to higher Peltier cooling. The material ZT were calculated from the three individual properties (that is, electrical resistivity, Seebeck coefficient and thermal conductivity) at T = 300 K. The observed module ZT of the CHES TFTEC device is higher than both bulk devices – translating to less energy consumed in the cooling sensation in the present study and higher heat-to-electric conversion efficiency in a related study²⁵.



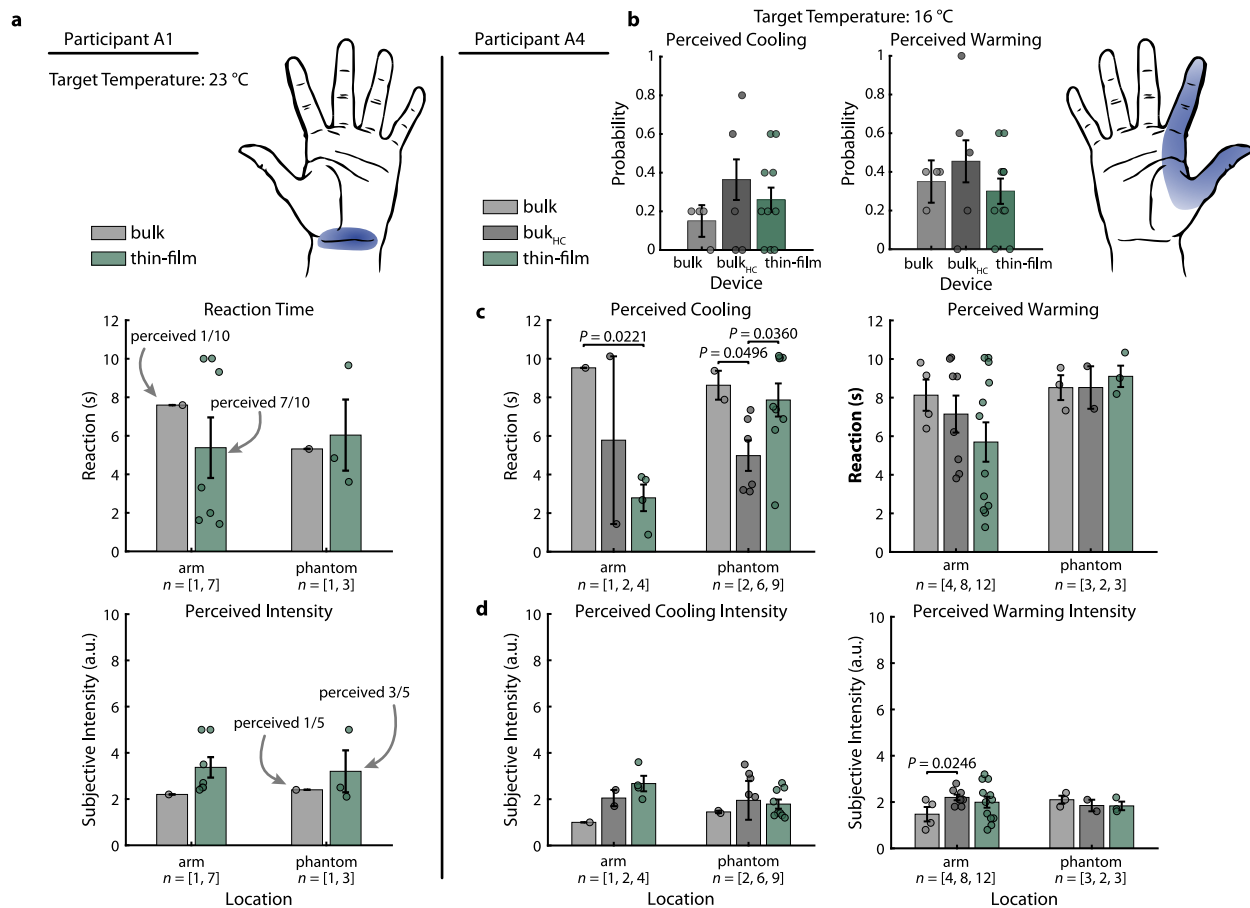
Extended Data Fig. 4 | Exemplar thin-film thermoelectric device cooling and repeatability. **a**, Cooling profile as a function of current for two example TFTEC devices with a $\Delta T_{\max} = 61.8^{\circ}\text{C}$ (305 K p-n couple Harman ZT of -0.72) and $\Delta T_{\max} = 68.7^{\circ}\text{C}$ (305 K p-n couple Harman ZT of -0.96) for Module 1 and 2, respectively. Unlike thinned bulk TE materials which can achieve a ΔT_{\max} up to 23°C ⁶⁶, modules with thin-film TE materials can result in ΔT_{\max} up to 68.7°C . **b**, The temperature differential (ΔT) is the difference between the hot side (T_{hot}) and the cold side (T_{cold}) of the TFTEC device during steady-state performance. **c**, Cooling reproducibility of the TFTEC device (Module 1) in (a) for 50 cycles over more than 400 min. Data points shown are the temperature differential between T_{hot} and T_{cold} at steady state after input current to the device was turned off ($\Delta T = 0^{\circ}\text{C}$) or on ($\Delta T = 62^{\circ}\text{C}$). Previous TFTEC devices were reported

to be stable over 500,000 cycles⁶⁷. **d**, Perceptual data was collected with one participant wearing the TFTEC device on the index finger over 3 hr. The reaction and perceived intensity of the thermal stimulation did not significantly change over the experiment and the participant perceived thermal sensations on every trial ($n = 45$ independent trials from one TFTEC device). Trend lines were fit using linear regression and the fitted slopes were not significantly different from zero ($P_{\text{slope}} > 0.05$), suggesting perceptual and hardware stability (that is, no significant changes in perception) while wearing the TFTEC device for the extended duration. Data are presented as individual measurements. A one-sample *t*-test, using the estimated regression slope and its standard error, were used to calculate the statistical *P* values for the regression slopes.



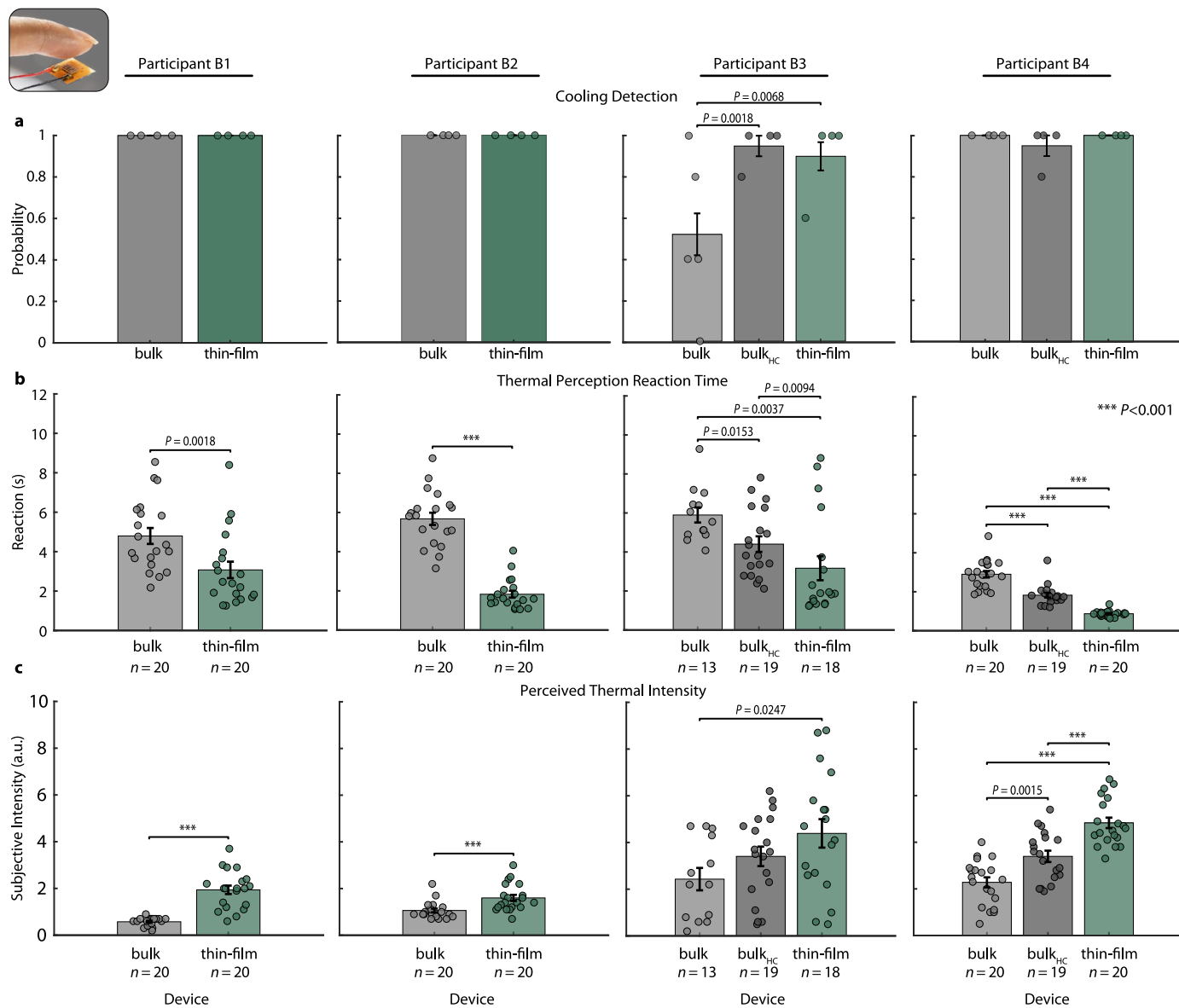
Extended Data Fig. 5 | Baseline visual reaction time. a, The amputee and non-amputee participants performed a visual reaction time task using the same button used in the thermal stimulation task. Data represents independent trials; $n = 30$ for A2, A3, and A4; $n = 90$ for B1 and B3; $n = 60$ for B2 and B4. **b,** Performance metrics. Participant A1 did not perform the visual reaction time task. The violin

plot whiskers represent the minimal and maximal values, the vertical lines indicate the first and third quartiles, the horizontal lines are means, and the white dots are the medians. The average reaction time for each non-amputee participant was used to normalize the thermal stimulation reaction time results and compare across individuals.



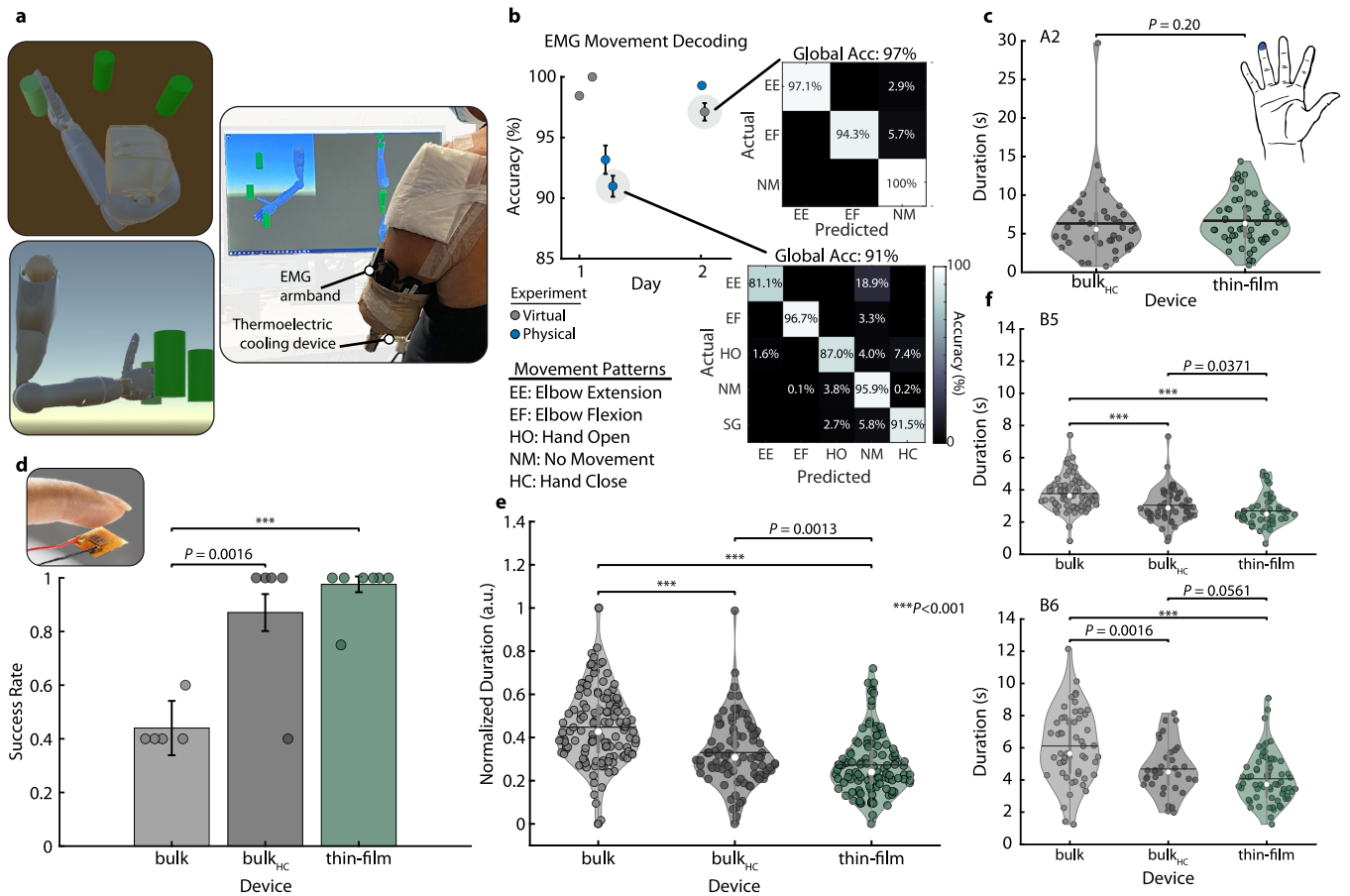
Extended Data Fig. 6 | Thermal reaction and perception in participants with limb amputation. **a**, Thermal detection experiment at 23 °C for participant A1. Statistical comparisons were not performed because only one trial was detected for the bulk device at each stimulation site. **b**, Participant A4 also performed the thermal detection experiment with the bulk_{HC} device and reported sensations of warming on some trials despite the target temperature being set to 16 °C (Supplementary Discussion). Data presented as performance per block of up to five independent trials, $n = 20$ trials (4 blocks, bulk), 22 trials (5 blocks, bulk_{HC}), and 50 trials (10 blocks, TFTEC). **c**, Thermal stimulation on the residual limb with the thin-film device leads to faster reaction times; however, the bulk_{HC} device was perceived faster on trials that were felt as cooling sensations in the phantom

hand. There were no significant differences across the devices on trials that were perceived as warming. **d**, Perceived intensity was similar across all devices and stimulation sites for this participant, with the exception of the thin-film device eliciting slightly stronger cooling sensations on the arm and the bulk_{HC} device eliciting slightly stronger sensations on trials perceived as warming. **a, c, d**, Number of independent trials for each condition that elicited thermal perception is given by n . Total number of independent trials, including those that did not elicit thermal perception, for each condition was 10 (A1 arm TFTEC); 5 (A1 bulk, phantom TFTEC); 10 (A4 bulk, arm bulk_{HC}); 12 (A4 bulk_{HC} phantom); and 25 (A4 TFTEC). Data represents independent trials and bars represent mean \pm s.e.m of individual trials. P values were generated with a two-sided Mann-Whitney U test.



Extended Data Fig. 7 | Detection, reaction, and perception of thermal stimulation for non-amputee participants. **a**, Probability of detecting cooling sensations in individual intact limb participants. Data presented as performance per block of five independent trials, $n = 20$ independent trials (4 blocks) for all conditions except for $n = 25$ independent trials (5 blocks) for B3 with the bulk device. **b**, Reaction time and **c**, perceived intensity of thermal stimulation,

n represents number of independent trials where cooling sensation was perceived. Data are presented from individual trials where cooling was perceived. The target temperature was set to 16 °C for all devices. In all instances, the thin-film device led to faster and more intense thermal perception during stimulation of the index fingertip. Bar plots are presented as mean \pm s.e.m. of individual trials, P values were generated with a two-sided Mann-Whitney U test.



Extended Data Fig. 8 | Cold object detection using thermal feedback for amputee and non-amputee participants. **a**, Participants controlled the vMPL using EMG (A1) or motion tracking (A2, B5, B6) with a wireless armband. Thermal feedback was provided to the phantom hand (amputee) or tip of the index finger (non-amputee). **b**, EMG decoding (A1). Only elbow movements were used for the virtual task. Data presented as mean \pm s.e.m. of $n = 5$ feature sets. **c**, The time spent touching each object during the virtual task for A2 was similar between $bulk_{HC}$ ($n = 40$ touches over 10 trials) and TFTEC ($n = 54$ touches, 15 trials) devices. **d**, The two non-amputee participants were more successful detecting virtual cold objects with the $bulk_{HC}$ ($n = 24$ trials, 5 blocks) and TFTEC ($n = 34$ trials, 7 blocks) device compared to the bulk device ($n = 25$ trials, 5 blocks). Bar plots represent mean \pm s.e.m.; data points represent blocks with up to five trials. **e**, For the two

non-amputee participants, the normalized time spent touching virtual objects was significantly shorter for the TFTEC ($n = 112$ touches, 34 trials) compared to the bulk ($n = 133$ touches, 25 trials) and $bulk_{HC}$ ($n = 92$ touches, 24 trials) devices. Data normalized using max-min normalization for each participant. **f**, Time spent touching each virtual object. For B5, $n = 80, 58,$ and 46 touches, over 15 trials with each device, for bulk, $bulk_{HC}$, and TFTEC, respectively. For B6, $n = 53, 34,$ and 66 touches for bulk (10 trials), $bulk_{HC}$ (9 trials), and TFTEC (19 trials), respectively. **c, e, f**, Data represent independent virtual object touches and all trials are independent. Violin plot whiskers represent the minimal and maximal values, vertical lines indicate first and third quartiles, horizontal lines are means, and white dots are the medians. P values were generated with a two-sided Mann-Whitney U test.

Reporting Summary

Nature Portfolio wishes to improve the reproducibility of the work that we publish. This form provides structure for consistency and transparency in reporting. For further information on Nature Portfolio policies, see our [Editorial Policies](#) and the [Editorial Policy Checklist](#).

Statistics

For all statistical analyses, confirm that the following items are present in the figure legend, table legend, main text, or Methods section.

n/a Confirmed

- The exact sample size (n) for each experimental group/condition, given as a discrete number and unit of measurement
- A statement on whether measurements were taken from distinct samples or whether the same sample was measured repeatedly
- The statistical test(s) used AND whether they are one- or two-sided
Only common tests should be described solely by name; describe more complex techniques in the Methods section.
- A description of all covariates tested
- A description of any assumptions or corrections, such as tests of normality and adjustment for multiple comparisons
- A full description of the statistical parameters including central tendency (e.g. means) or other basic estimates (e.g. regression coefficient) AND variation (e.g. standard deviation) or associated estimates of uncertainty (e.g. confidence intervals)
- For null hypothesis testing, the test statistic (e.g. F , t , r) with confidence intervals, effect sizes, degrees of freedom and P value noted
Give P values as exact values whenever suitable.
- For Bayesian analysis, information on the choice of priors and Markov chain Monte Carlo settings
- For hierarchical and complex designs, identification of the appropriate level for tests and full reporting of outcomes
- Estimates of effect sizes (e.g. Cohen's d , Pearson's r), indicating how they were calculated

Our web collection on [statistics for biologists](#) contains articles on many of the points above.

Software and code

Policy information about [availability of computer code](#)

Data collection

Sensory maps drawn by participants were recorded on printed sheets of paper with hand outlines, and sensory perceptions from stimulation were recorded by colour-coding the sensory maps on the same printed sheet of paper. The data were digitized using a commercial office document scanner. Data from benchtop thermoelectric-device characterization were collected using a commercial video camera and recorded manually into a lab notebook and Microsoft Excel 2016 spreadsheet. Thermal stimulation data were recorded through a custom-made software written in MATLAB R2018b. Reaction and perceived intensity data were recorded through a custom-made software written in MATLAB R2018b. The closed-loop thermal feedback experiments were implemented using custom software, written in MATLAB R2022a, to interface with the virtual and physical prostheses while recording trial data, including thermal stimulation, prosthesis movements and sensing, trial completion and timestamps. The Virtual Integration Environment software architecture, which is available at <https://bitbucket.org/rarmiger/minivie>, was used to control the virtual and physical Modular Prosthetic Limbs. Videos of participants were recorded using a Canon VIXIA HF G20. Infrared temperature images and video were recorded using a Jenoptik VairoCAM HD camera.

Data analysis

The data were analysed and plotted using MATLAB R2018b and R2022a. The figures were prepared using Adobe Illustrator 2021 and Adobe Illustrator 2022. The videos were prepared using Adobe Premiere Pro 2021 and Premiere Pro 2022. Thermogram image analysis was performed using IRBIS 3 Professional.

For manuscripts utilizing custom algorithms or software that are central to the research but not yet described in published literature, software must be made available to editors and reviewers. We strongly encourage code deposition in a community repository (e.g. GitHub). See the Nature Portfolio [guidelines for submitting code & software](#) for further information.

Data

Policy information about [availability of data](#)

All manuscripts must include a [data availability statement](#). This statement should provide the following information, where applicable:

- Accession codes, unique identifiers, or web links for publicly available datasets
- A description of any restrictions on data availability
- For clinical datasets or third party data, please ensure that the statement adheres to our [policy](#)

All source data generated or analysed during the study and needed to interpret and verify the findings are available within the paper and its Supplementary Information. Source data for the figures are provided with this paper.

Field-specific reporting

Please select the one below that is the best fit for your research. If you are not sure, read the appropriate sections before making your selection.

- Life sciences Behavioural & social sciences Ecological, evolutionary & environmental sciences

For a reference copy of the document with all sections, see [nature.com/documents/nr-reporting-summary-flat.pdf](https://www.nature.com/documents/nr-reporting-summary-flat.pdf)

Life sciences study design

All studies must disclose on these points even when the disclosure is negative.

Sample size	<p>No statistical methods were used to predetermine the number of participants because this was a proof-of-concept study.</p> <p>The number of repetitions to perform and verify the sensory mapping results was based on prior results and mapping procedures described in Osborn et al., <i>Sci Rob</i> 2018 and Osborn et al., <i>J Neural Eng</i> 2020.</p> <p>The number of trials for each group during thermal reaction time testing were based on a prior study measuring similar perceptual responses (Lele and Sinclair, <i>J Neurol Neurosurg Psychiat</i>, 1955).</p> <p>The number of trials for the visual-reaction experiment was based on prior studies (Jain et al., <i>Int J Appl Basic Med Res</i>, 2015 and Barrett et al., <i>Sci Rep</i>, 2020).</p> <p>The duration of the extended perceptual experiment was based on a prior study testing a wearable sensory stimulation for 3 h of continuous use (Seim et al, <i>J Neuroeng Rehab</i>, 2021).</p> <p>The number of repetitions to perform the functional closed-loop thermal feedback experiments was based on prior prosthesis-related functional experiments reported in in Osborn et al., <i>Sci Rob</i> 2018 and Osborn et al., <i>J Neural Eng</i> 2020.</p>
Data exclusions	<p>An additional non-amputee participant consented to participate, but owing to technical issues did not complete the study. Their data are not reported and were excluded from the analyses. One amputee participant performed one block of the virtual-prosthesis functional task with thermal feedback to another site on their phantom hand; these data were not included because the placement of the thermal stimulator on the skin did not make sufficiently good contact to provide thermal transfer to the skin. One amputee participant performed one trial of the physical-prosthesis functional task where the thermal feedback was not delivered; these data were not included because the trial was ended owing to the technical issue.</p>
Replication	<p>Multiple trials were conducted on the same day. with each participant for the thermal-reaction-time and cold-object identification experiments. For the thermal-reaction-time experiment, participants A1, A2, A3 and A4 performed 20, 30, 30 and 20 trials with the bulk device, respectively; they performed 25, 30, 34 and 50 trials with the thin-film device, respectively; and participant A4 performed 22 trials with the high-capacity bulk device. For the visual-reaction-time experiment, amputee participants –A4) performed 30 trials and non-amputee participants B2 and B4 performed 60 trials; B3 and B4 performed 90 trials. For the physical-cold-object-detection experiment, participant A1 performed 19 trials with the thin-film device. For the extended thermal-perception experiment, participant B2 performed the entire experiment once and performed 45 trials over 3 hours. For the virtual-cold-object-detection experiment, participant A1 performed 15, 10 and 31 trials with the bulk, high-capacity bulk and thin-film devices, respectively. Participant A2 performed 10 and 15 trials with the bulk and thin-film devices, respectively. Participants B5 and B6 performed 25, 24 and 34 trials with the bulk, high-capacity bulk and thin-film devices. All attempts at replication within participants and across participants were successful.</p>
Randomization	<p>The participants performed the same tests in the same conditions. During the thermal-stimulation experiments with different devices, we randomized the ordering of the device-stimulation blocks. Combined participant results were compared across the same device. The investigators were not blinded to the randomization order.</p>
Blinding	<p>The investigators were not blinded to allocation during experiments and assessments. Given the perceptual nature of the experiments, the participants were generally aware of when they were being stimulated, preventing us from providing stimulation without their knowledge. The participants were not aware of any explicit changes made to the stimulation, and were not prompted as to what type of sensation they should experience. The validity of the results are not biased by the participant's knowledge because they were not aware of when changes were made to stimulation and because objective measures (such as reaction time) were also measured in addition to perceived experiences.</p>

Reporting for specific materials, systems and methods

We require information from authors about some types of materials, experimental systems and methods used in many studies. Here, indicate whether each material, system or method listed is relevant to your study. If you are not sure if a list item applies to your research, read the appropriate section before selecting a response.

Materials & experimental systems

n/a	Involvement in the study
<input checked="" type="checkbox"/>	<input type="checkbox"/> Antibodies
<input checked="" type="checkbox"/>	<input type="checkbox"/> Eukaryotic cell lines
<input checked="" type="checkbox"/>	<input type="checkbox"/> Palaeontology and archaeology
<input checked="" type="checkbox"/>	<input type="checkbox"/> Animals and other organisms
<input type="checkbox"/>	<input checked="" type="checkbox"/> Human research participants
<input checked="" type="checkbox"/>	<input type="checkbox"/> Clinical data
<input checked="" type="checkbox"/>	<input type="checkbox"/> Dual use research of concern

Methods

n/a	Involvement in the study
<input checked="" type="checkbox"/>	<input type="checkbox"/> ChIP-seq
<input checked="" type="checkbox"/>	<input type="checkbox"/> Flow cytometry
<input checked="" type="checkbox"/>	<input type="checkbox"/> MRI-based neuroimaging

Human research participants

Policy information about [studies involving human research participants](#)

Population characteristics

Upper-extremity amputation (participants A1–A4) and no-upper-extremity amputation (participants B1–B6). Participant A1 was a male with a left transhumeral amputation, targeted-muscle-reinnervation surgery, and an osseointegrated implant. Participant A2 was a male with a right transradial amputation. Participant A3 was a female with a right transradial amputation and a left partial hand amputation. Participant A4 was a female with a right transhumeral amputation and had undergone targeted-sensory-reinnervation surgery. Participants A1–A4 had an age range of 41–65 years old (mean: 52 years old). Participants B1–B6 included three males and three females with no limb amputation (age range: 20–30 years old, mean: 24.8 years old).

Recruitment

The participants with amputation were recruited from a population of upper-extremity amputees that were part of previous studies (Osborn et al., J Neural Eng, 2020; Osborn et al., IEEE Biomed Circ Syst Conf, 2017) or who were referred to the study by local clinicians. The participants without amputation were recruited from the Johns Hopkins University Applied Physics Laboratory (JHU/APL) through advertisements. Participants were compensated up to \$15 per hour in gift cards, or if participants were JHU/APL employees then they were given a project budget to cover their time for performing the experiments.

Ethics oversight

Johns Hopkins Medicine Institutional Review Boards.

Note that full information on the approval of the study protocol must also be provided in the manuscript.